EVALUATION OF FLUSH-MOUNTED HOT-FILM SENSORS USED FOR THE MEASUREMENTS OF SKIN FRICTION

by

TAI HUAT DANG

A thesis
presented to the University of Manitoba
in partial fulfillment of the
requirements for the degree of
MASTER OF SCIENCE
in
Department of Mechanical Engineering

Winnipeg, Manitoba

ISBN 0-315-37191-9

EVALUATION OF FLUSH-MOUNTED HOT-FILM SENSORS USED FOR THE MEASUREMENTS OF SKIN FRICTION

BY

TAI HUAT DANG

A thesis submitted to the Faculty of Graduate Studies of the University of Manitoba in partial fulfillment of the requirements of the degree of

MASTER OF SCIENCE

I hereby declare that I am the sole author of this thesis.

I authorize the University of Manitoba to lend this thesis to other institutions or individuals for the purpose of scholarly research.

T.H. DANG

I further authorize the University of Manitoba to reproduce this thesis by photocopying or by other means, in total or in part, at the request of other institutions or individuals for the purpose of scholarly research.

T.H. DANG

ABSTRACT

To prove the assumption of fully developed turbulent pipe flow, measurements for skin friction, mean velocity profiles and various higher-order moments of fluctuating velocity have been made at tunnel length to diameter ratios of L/D = 78 and 98 in the Reynolds numbers of 1.14×10^5 and 2.31×10^5. The invariability of these measurements at both axial positions prove that the flow is fully developed beyond L/D = 78.

Three different types of hot-film probes, namely the DISA-55A92 and TSI-1237 flush-mounted hot-film probes and the DISA-55R47 glue-on probe, were calibrated in the fully developed pipe flow. The correction method used to account for temperature drift in the tunnel is described. An air gauge was modified and built to assist in positioning the flush-mounted hot-film probes. It was shown that all three probes tested confirm the usual 1/3-power law. Attempts were made to determine skin friction values in the developing flow region by using the glue-on probe previously calibrated in fully developed turbulent flow.

Further, by mounting the hot-film probes on different pipe materials, such as steel, aluminium, red brass and copper, the effect of the thermal conductivity of the various pipe materials on the hot-film probes was investigated.

ACKNOWLEDGEMENTS

The author would like to express his appreciation to his thesis advisor, Dr. R.S. Azad for his guidance and many beneficial discussions in this work. Gratitude is expressed to K. Tarte for his assistance in the equipment set-up and the preparation of the figures. Further, the author is indebt to L.G. Ozimek and Brian Doell for reading the original manuscript.

Special thanks are due to my parents and my wife for their patience and encouragements.

TABLE OF CONTENTS

	Page
ABSTRACT	I
ACKNOWLEDGEMENTS	III
TABLE OF CONTENTS	IV
LIST OF FIGURES	VI
LIST OF TABLES	IX
NOMENCLATURES	X
1. INTRODUCTION	1
2. LITERATURE REVIEW	4
2.1 Ludwieg, Ludwieg and Tillman	4
2.2 Liepmann and Skinner	5
2.3 Bellhouse and Schultz	6
2.4 Geremia	7
2.5 Pardo	8
3. EXPERIMENTAL FACILITIES	10
3.1 Wind Tunnel	10
3.1.1. Wind Tunnel Calibration	12
3.2 Instrumentations	13
3.2.1 Pressure Measuring Devices	13
3.2.2 Hot Wire Probes	14
3.2.3 Hot Film Probes	16

Page

4. FLUSH-MOUNTED HOT FILM PROBES CALIBRATION TECHNIQUE 19

4.1 Positioning of Probes 19

4.1.1 The Air Gauge Technique 20

4.2 Mounting of Glue-On Probe 21

4.3 Temperature Sensitivity 23

4.4 Probe Calibration 25

5. RESULTS AND DISCUSSIONS 31

5.1 Fully Developed Turbulent Pipe Flow . . . 31

5.2 Hot Film Probe Calibration 37

6. CONCLUSIONS 43

7. RECOMMENDATIONS 45

8. REFERENCES 46

APPENDIX I: AIR GAUGE DESIGN 49

TABLES 50

FIGURES 60

LIST OF FIGURES

Figure		Page
1	Layout of wind tunnel	60
2	Velocity profile before the installation of flexible coupling	61
3	Velocity profile after the installation of flexible coupling	62
4	Wind tunnel calibration plot	63
5	Hot-wire data acquisition system	64
6	DISA subminiature flush-mounted hot-film probe	65
7	Thermo-Systems flush-mounted hot-film probe	66
8	DISA glue-on probe	67
9	Hot-film probe support	68
10	Air gauge design	69
11	Effects of metal-metal and metal-plastic joints	70
12	Shear stress calibration curve for metal pipes	71
13	Hot-film sensor circuit	72
14	Ratio of U_b/U_c and $U_{3/4}/U_b$	73
15	Velocity profile at L/D = 78 and L/D = 98 for Re = 1.14×10^5 and Re = 2.31×10^5 . .	74
16	Skin friction coefficient versus Reynolds number	75
17	Distribution of static pressure for metal pipes	76
18	Non-dimensional velocity distribution: plot obtained with pitot tube	77

Figure		Page
19	Skewness distribution of the longitudinal velocity, u, $S(u) = \overline{u^3}/(\overline{u^2})^{3/2}$	78
20	Moments of turbulent fluctuating velocity in fully developed pipe flow	
	a) $\overline{w^2}/(\overline{u^2} + \overline{v^2})$ b) $\overline{vw^2}/(\overline{u^2 v} + \overline{v^3})$ . . .	79
21	Fluctuating velocity distributions at L/D = 78 and L/D = 98 for Re = 1.14×10^5 .	80
22	Fluctuating velocity distributions at L/D = 78 and L/D = 98 for Re = 2.31×10^5 .	81
23	Shear stress measurements at L/D = 78 and L/D = 98 for Re = 1.14×10^5 and 2.31×10^5	82
24	Profile of the correlation coefficient $\overline{uv}/u'v'$ across the pipe flow	83
25	Distribution of $\overline{vq^2}/U_b^3$	84
26	Calibration curve for DISA-55R47 hot-film probe on steel pipe	85
27	Calibration curve for DISA-55A92 hot-film probe mounted on steel pipe	86
28	Calibration curve for DISA-55A92 hot-film probe mounted on red brass pipe	87
29	Calibration curve for DISA-55A92 hot-film probe mounted on copper pipe	88
30	Calibration curve for DISA-55A92 hot-film probe mounted on aluminium	89
31	Calibration curve for DISA-55A92 hot-film probe mounted on steel pipe - Test #2 . . .	90
32	Calibration curve for TSI-1237 hot-film probe mounted on steel pipe	91
33	Calibration curve for TSI-1237 hot-film probe mounted on red brass pipe	92

Figure		Page
34	Calibration curve for TSI-1237 hot-film probe mounted on copper pipe	93
35	Calibration curve for TSI-1237 hot-film probe mounted on aluminium pipe	94
36	Calibration curve for TSI-1237 hot-film probe mounted on steel pipe - Test #2 . . .	95
37	Shear stress distribution along pipe length	96
38	Skin friction distribution along pipe length	97

LIST OF TABLES

Table		Page
1	Different types of pipe used in the calibration of hot-film probes	50
2	Calculation of $\frac{U^*l}{\nu} < 64\ Pr$ for various probes	51
3	Hot-film calibration data for DISA-55R47 mounted on steel pipe	52
4	Hot-film calibration data for DISA-55A92 mounted on aluminium pipe	53
5	Hot-film calibration data for DISA-55A92 mounted on red brass pipe	54
6	Hot-film calibration data for DISA-55A92 mounted on copper pipe	55
7	Hot-film calibration data for TSI-1237 mounted on red brass pipe	56
8	Hot-film calibration data for TSI-1237 mounted on aluminium pipe	57
9	Hot-film calibration data for TSI-1237 mounted on steel pipe	58
10	Hot-film calibration data for TSI-1237 mounted on copper pipe	59

NONCLAMENTURE

A,B	Hot-film calibration constants
BP	Measured barometric pressure
C_f	Skin friction coefficient $[2\ (U^*/U_\infty)^2]$
C_p	Specific heat of fluid
d_1	Diameter of orifice
d_2	Diameter of air gauge outlet
D	Inside diameter of pipe (10.16 cm)
E_b	Bridge voltage of hot-film anemometer circuit
i	Probe current
l	Length of probe normal to flow
Nu	Nusselt number
Pe	Peclet number
Pr	Prandtl number
P_s	Local static pressure
q^2	Twice the turbulent kinetic energy $(\overline{u^2} + \overline{v^2} + \overline{w^2})$
r	Radial distance from axis
R	radius of pipe
Re	Reynolds number $(U_b D/\nu)$
ΔT	Difference between the probe operating temperature and the fluid temperature
u	Fluctuating axial velocity
U	Local mean axial velocity
U_b	Bulk velocity
U_c	Centreline velocity

U^+	Dimensionless local mean velocity (U/U*)
U^*	Friction velocity
v	Fluctuating transverse or radial velocity
V	Mean radial velocity
w	Fluctuating circumferential velocity
x	Axial distance in the streamwise direction
y	Radial distance in the streamwise direction
y^+	Dimensionless position (YU^*/ν)
δ	Boundary layer thickness
λ	Fluid thermal conductivity
ν	Kinematic viscosity
ρ	Fluid density
τ_w	Wall shear stress

CHAPTER 1

INTRODUCTION

The hot-wire anemometer is generally accepted as one of the most popular devices used to obtain measurements of flow parameters. However, in situations when measurements very close to a wall have to be made, the hot-wire anemometer over-estimates the value of the flow velocity. As distance to the wall decreases and flow velocity or flow Reynolds number increases, this deviation from the true response becomes more pronounced. The distance between the hot-wire and the wall, the flow velocity, aerodynamic effects near the wall, the thermal nature of the wall material, and the calibration of the anemometer all influence anemometer readings in the vicinity of the wall.

Another instrument, the hot-film anemometer, has a special application for making turbulence measurements very close to the wall within the viscous sublayer. Due to the highly turbulent nature of the airflow under study, a better understanding of the heat transfer rate to the fluid, and the effect of heat conductivity for different pipe materials is needed.

The idea of a built-in wall sensor has been around since the 1950's. The technique of measuring wall shear stresses in boundary layer flows using flush-mounted hot-film probes has been utilized by, among others, Ludwieg (1950), Liepmann & Skinner (1954), and Bellhouse and Schultz (1966). The hot-film probe consists of a thin metallic film baked onto a non-conductive substrate. The film forms one arm of the constant temperature anemometer bridge. An electric current is continuously supplied to the hot-film through a high feedback amplifier in order to maintain the hot-film at a constant temperature higher than that of ambient fluid. Providing the thermal boundary layer generated by the heated film is less than the viscous sublayer of the turbulent boundary layer, the resulting heat transfer rate Q_t to the fluid can be related to the wall shear stress τ_w as

$$\tau_w \propto Q_t^3$$

Basic characteristics of hot-film probes have been detailed by Geremia (1970). The major advantages of using a hot-film probe are that it does not disturb the flow as does the Preston tube, it is mechanically simple, and it measures shear stress at a point in comparison to movable element shear stress sensor which measures sheer stress over a large area.

The present study deals with the calibration and evaluation of the different types of flush-mounted hot-film probes that are available commercially. Pipes of different material having different heat conductivity were chosen to see how the flush-mounted hot-film probe output is affected by those pipes. Based on the calibration curves obtained from the fully developed region, measurement of skin friction in the developing flow region were attempted. Temperature sensitivity correction and positioning of the probes are also described.

In addition, before work on the hot-film calibration curves could proceed, it was necessary to show that the tunnel flow under consideration was fully developed pipe flow. Mean velocity fluctuating quantities up to the third order were measured at non-dimensional distances L/D = 78 and L/D = 98 to check for invariability between the two axial positions. These measurements were performed in the Reynolds numbers of 1.14×10^5 and 2.31×10^5.

CHAPTER 2

LITERATURE REVIEW

2.1 Ludwieg, H. (11) and Ludwieg, H. and Tillmann, W. (1950)

Ludwieg (1950), using a small, heat conducting metal block, attempted to reduce the shear stress measurement to a heat transfer measurement. The metal block was inserted in the solid wall and a small electric heater was used to raise the temperature of the block above that of the fluid and the solid wall. The author showed that the relationship between the shear stress and heat transfer could be expressed as

$$Nu \propto \tau_w^{1/3}$$

or

$$\frac{i^2R}{\Delta T} \propto \tau_w^{1/3}$$

The friction coefficients, and hence the shear stress, were computed based on the test data obtained by Schultz-Grunow (1941). The other terms, namely, i^2R and ΔT, could be easily measured during calibration. The experimental results gave the approximate linear variation of the calibration curve which is largely attributable to the presence of the celluloid diaphragm between the surface of the copper block and the flowing air.

Using the same instrument, Ludwieg and Tillmann (1950) studied the wall shear stress of the boundary layers in channel flows under different pressure gradient conditions. The instrument was calibrated using plate flow and the corresponding calibration shear stress was evaluated using the Schultz-Grunow formula. The authors pointed out that for general turbulent boundary layers in the wall proximity, that is in the viscous sublayer, in the transition zone, and in the part of the completely turbulent zone near the wall, the same universal law applies as for the plate flow. Consequently, the related friction coefficient C_f can then be determined simply from the known velocity profile.

2.2 The Liepmann and Skinner Hot-Wire Experiment (1954)

Liepmann and Skinner (1954) studied both laminar and turbulent flow over a flat plate by mounting a hot-wire cemented into a groove in the surface of a hard rubber ebonite plate. The authors showed that for a single calibration of the probe to be applicable for both laminar and turbulent flow, the thermal boundary layer thickness must be smaller than the viscous sublayer thickness of the turbulent boundary layer. The authors showed, using dimensional analysis, that

$$Nu\ (L, \xi) \propto (PrC_f R_\xi^2 \frac{L^2}{\xi})^{1/3}$$ where

L = effective wire length

ξ = x-coordinate of the upstream edge of the heated element

R = Reynolds number based on ξ .

For a given set of conditions, this equation reduces to

$$\frac{i^2R}{\Delta T} = A\tau_w + B$$

Where i is the current, R the resistance, and τ_w the wall shear stress.

The shear stress was calculated from the slope of the velocity profile in the sublayer. The scatter in their results could largely arise from the proximity of the hot wire to the wall.

2.3 Bellhouse, B.J. and Schultz, D.L. (1966)

Bellhouse, B.J. and Schultz, D.L. studied the laminar and turbulent flow on a flat plate, circular cylinder, and annular tunnel. The results confirm the 1/3 power equation:

$$\frac{i^2R}{\Delta T} = A\tau_w + B$$

However, for the turbulent flow, in order for the above equation to hold, the thermal-layer thickness must be less than the viscous sublayer. The value of $i^2R/\Delta T$ can be

experimentally measured during calibration. The wall shear stress τ_w, can be obtained from theoretical solutions.

For a circular cylinder, τ_w was determined from a theoretical solution based on the work of Fage and Falkner (1930). For an annulus, the authors state that provided the flow is uniform, it can be shown that $\tau_w^{1/3} = 6.284 \times 10^{-2} (\Delta P)^{1/3}$ where ΔP is the pressure drop in psi over a 72.5 inch length of tunnel. In the case of flat plate measurements, the skin friction coefficient can be calculated in laminar and turbulent flow using either 1/2 or 1/5 power laws of Reynolds number respectively.

2.4 Geremia, J.O. (1970)

This author presented a method of calibrating flush-mounted fibre sensors for wall shear stress in water. The calibration of the flush-mounted hot-film anemometers was carried out using a 40 foot 4 inch diameter stainless steel pipe. Making use of the known shear stress in a fully developed pipe flow, the author demonstrated that the hot-film probe can be calibrated very accurately and precisely provided it is carefully mounted. However, it was found that for calibration of the flush-mounted hot-film anemometers on a flat plate, the local skin friction data is some twenty times less accurate. It was also found that the

probe calibration could be carried over to another apparatus provided the shear stress range was approximately the same and provided the thermal layer is much thinner than the viscous sublayer.

2.5 Pardo, D.F. (1980)

In this study, the author devised a solution scheme to solve the two-dimensional heat transfer problem consisting of an isothermal heated strip mounted on an isotropic thermally conducting substrate subjected to laminar, steady flow over its surface. It was found that the heat transfer into the fluid above the heated strip is a function of the Peclet number, but is virtually independent of the thermal conductivity ratio. Heat flux into the substrate is highly dependent upon the thermal conductivity ratio but is independent of the Peclet number. Based upon the heat flux data generated by the computer program, the author stated that the general equation for the Nusselt number of total heat transfer can be written as

$$Nu = 0.66\ (k_s/k_f) + 0.76\ Pe^{1/3}$$

where k_s is the thermal conductivity of substrate, k_f is the thermal conductivity of fluid and Pe is the Peclet number.

Virtually all the findings of the earlier research supports the 1/3-power law. Liepmann and Skinner (1954), in their hot-wire experiment, also investigate the conditions under which a single calibration is sufficient for the probe to be applicable in both laminar and turbulent flow. Geremia (1970) also investigated the condition under which the calibration can be carried over to another apparatus. However, the problem of the effect of the thermal conductivity of the pipe material on the various types of hot-film probes has yet to be examined.

CHAPTER 3

EXPERIMENTAL FACILITIES

3.1 Wind Tunnel

The study of the fully developed pipe flow and the calibration of the shear stress probes were carried out in an open-return type wind tunnel. This tunnel has been described by Azad and Hummel (1971). Figure 1 shows the detailed layout of the wind tunnel. The test section for the fully developed pipe flow consisted of several sections of steel pipes having inside diameter of 0.1016 m (4.0 inches). However, a slight modification was made on the tunnel for the present study. A flexible coupling 70 x 34 x 27 cm was added between the rectangular-to-circular duct section and the screen section in an attempt to further reduce induced vibrations. It was initially thought that the installation of the flexible coupling might have an effect on the flow in the tunnel. To dispel this doubt, the velocity distribution across the diameter of the pipe was measured at several Reynolds numbers, before and after the installation of the flexible coupling. Comparison of Figure 2, showing velocity profile before the flexible coupling was installed; and Figure 3, showing the velocity profile after the flexible coupling was installed, did not reveal any

changes and simply confirmed that the velocity profile is independent of the equipment upstream of the contraction cone. Measurements of the fully developed pipe flow were taken at two different test positions, ie. at the test pipe length of seventy-eight pipe diameters and ninety-eight pipe diameters. To avoid end effects, the measuring station was located at one pipe diameter from the pipe exit for hot-wire and hot-film studies. The calibration of the shear stress probes was carried out at seventy-eight pipe diameters using pipes made of different materials but with the same inside diameter of 0.1016m (4.0 inch). Table 1 lists the physical properties of the different test sections used in the calibration of the hot-film probes.

The hot-wire probes could be manoeuvered within the pipe or outside the pipe using a traversing mechanism which has been described by Burhanuddin (1980). Initial positioning of the probes involved using a sensitive ohmmeter (Honar KRT 101 or ELC 068). The ohmmeter was activated when the hot-wire prongs made contact with the wall and the electrical circuit was completed.

At every point where the pipe touched the supports, a rubber pad was inserted to dampen the vibration. Static pressure taps of 1.0 mm diameter, spaced 90° apart around the pipe circumference, were drilled along the working pipe

section. The taps were joined to form a static pressure ring by using plastic tubing. The rings are spaced equally at intervals of 1.0 m. A total of four sets of piezometric rings were distributed along the test section. Following preston's (1950) recommendation, the last set was located at 0.5 diameter from the pipe exit. The pressure drop was measured over a distance of 4.0 m between the first and the last piezometric ring. The measurements were taken using a Betz manometer. A long tubing was used to join the pressure ring to the manometer in an effort to minimize the pressure fluctuations.

3.1.1 Wind Tunnel Calibration

The required free stream velocities were obtained by adjusting the power supply to the fan with a "Varimag" power control, and measuring the pressure drop across the tunnel contraction cone. The pressure drop was calibrated with the pitot tube in terms of centreline mean velocity or pipe bulk velocity. The calibration curve for the wind tunnel is plotted in Figure 4. The bulk velocities were obtained by integration of the velocity profiles measured at different tunnel operating points. The velocity profiles, in turn, are obtained from the total and wall static pressure measurements using Bernoulli's equation:

$$U = \sqrt{\frac{2}{\rho}(P_T - P_S)}$$

where P_T is the total or stagnation pressure and P_S the wall static pressure. It can be seen that both pipe bulk velocity and centreline velocity are proportional to the square root of the contraction cone pressure drop. These calibration curves are in close agreement with those previously obtained in the same tunnel by Kassab (1986).

3.2 Instrumentation

3.2.1 Pressure Measuring Devices

The velocity measurements for the calibration of hot-wire probes were obtained with wall static pressure and a United Sensor pitot tube which has a flattened tip and outer diameter of 1.2 mm. The closest point to the wall at which the measurement can be made using this tube was 0.15 mm. A Betz projection manometer with graduation of 0.1 mm of water and a range from -17 mm to 400 mm water was used for static and pitot pressure measurements. Similar results were obtained when a Combist micro-manometer and MKS Baratron Type 223 B pressure transducer were used. The Combist micro-manometer had graduation of 0.01 mm of water and range from 0-30 mm of water.

3.2.2 Hot-Wire Probes

The hot-wire probes used were a standard DISA-55P05 gold plated single wire probe and a DISA-55P51 gold plated X-wire probe. They have a 1.2 mm wire length and 5.0 mm wire diameter. The basic anemometer circuit is a DISA-55M01 constant temperature system, along with a DISA-55M25 linearizer.

The single wire and X-wire probes were calibrated in situ at the axis of the test pipe and operated at an overheat ratio of 0.8 in the constant temperature mode. A square wave test was carried out to ensure that the optimum frequency response was obtained. The hot-wires were calibrated daily prior to actual experimentation. In view of significant changes in probe calibration due to changes in ambient temperature, checks of the probe calibration were performed several times during a single run. The linearized outputs from the X-wire probes were matched to within 1.5% over the required operation range. The thermal stability of the electronic equipment was maintained by allowing the units to remain powered during the course of the experimental work even when the instruments were not in operation.

For all the measurements, the standard procedure recommended in the DISA technical literature was followed to obtain the linearized turbulence signal from the single and X-wire probes. The circumferential velocity component, w, was obtained by rotating the X-wire probe on its axis by 90° from the u-v plane. The vw component was similarly obtained by aligning the X-wire probe at 45° to both the x-y and x-z planes.

A DISA-55D31 integrating digital voltmeter, in conjunction with a Lab-chron timer was used to obtain a stable mean velocity reading. The rms fluctuating signal was measured by means of a DISA-55D35 rms voltmeter. The signals were monitored on the Tektronix 466 storage oscilloscope and adjusted for under- and over-amplification. The linearized anemometer output signal was fed into the Tri-met turbulence processor wherby all possible combinations of the u-component and v-component of the flow, up to the fourth order, can be formed. Simultaneous output signals may be taken three at a time depending on the function setting. The outputs from the turbulence processor were instantaneous values and were averaged over a period of 100 seconds using an LS7517 integrator before the signal was fed into a Hewlett Packard 3468A multimeter. The block diagram for the hot-wire data acquisition system is shown in Figure 5.

3.2.3 Hot-Film Probes

The hot-film probes used were a DISA-55A92 flush-mounted probe, a TSI-1237 flush-mounted probe, and a DISA-55R47 glue-on probe. Detailed descriptions of the various probes used can be found in this section.

The hot-film probes are used in conjunction with a DISA-55M01 constant temperature anemometer. The anemometer system heats the external sensor to a temperature greater than that of the ambient fluid temperature as determined by a selected overheat ratio. The sensitivity of the sensor increased with higher overheat ratios. However, too high an overheat ratios may damage the sensor. After some literature search, it was decided to use an overheat ratio of 0.6 for the present study.

The DISA-55A92 subminiature flush-mounted hot-film probe used in the study consists of 0.75 x 0.15 mm nickel film sputtered onto the flat end of cylindrical quartz rod. The film is protected by a 0.5 mm quartz coating and is designed for use in a non-conducting fluids. The probe is shown in Figure 6.

The second type of probe used is the Thermo-System Inc. TSI-1237 flush-mounted hot-film probe, shown in Figure 7. The sensor element is a platinum film strip, 0.127 x 1.0 mm, sputtered onto the flat end of cylindrical quartz rod. The film, unlike the DISA probe, is protected by a thin alumina coating. The surface is smooth and flush to within 0.025 mm.

Figure 8 shows the third type of probe used in this study, a DISA-55R47 glue-on probe. The sensor is a 0.1 x 0.9 mm nickel film deposited on a 0.05 mm thick polyimid foil. The film is protected by a 0.5 mm quartz coating. Unlike the flush-mounted hot-film probe, it is glued onto the wall and becomes a permanent fixture of the wall.

Caution must be used when calibrating the hot-film probe in a circular pipe due to the surface discontinuity between the curved pipe and the flat sensor which can create secondary currents that affect the actual shear stress. Positioning of the probes is described in section 4.1.

A total of six different types of pipe materials were planned for the calibration of hot-film probes. The details of the pipe description are presented in Table 1.

Holes for housing the hot-film probes were drilled perpendicular to the local area of the measurement point. Franklin and Wallace (1970) stated that large errors can occur if the drilled hole has burrs or other imperfections. Consequently, burrs resulting from the drilling process were eliminated using fine emery paper. The pipes were then cleaned with a compatible cleaning compound, rinsed thoroughly and dried before any test was performed.

CHAPTER 4

FLUSH-MOUNTED HOT-FILM PROBE CALIBRATION TECHNIQUE

4.1 Positioning of Probes

The hot-film probes used in this study are shown in Figures 6 to 8 inclusive. A possible discontinuity due to misalignment of the probe depth, can exist between the probe and the inside surface of the pipe. This discontinuity is inversely proportional to the radius of curvature of pipe.

The effect of the discontinuity can be noticed by moving the sensor inward and outward at the calibration test hole. It was found that by moving the probe towards the flow, the output voltage from the anemometer increases indicating a larger apparent shear stress value. Withdrawing the probe from the flow has the opposite effect. Pessoni (1974) found that displacement of a commercial probe from the test-section surface by 0.1 mm in a 2.5 cm air tunnel resulted in 30 to 40% deviations in the calibrations. Therefore, great care must be exercised in aligning the probe with the curved surface of the pipe such that the protrusion of the probe lies within an order of magnitude less than the calculated sublayer thickness. This alignment can be achieved using the air gauge technique

described by Geremia (1970).

In the present study, the technique employed by Geremia was modified slightly. The hot-film probe is attached to a micrometer as shown in Figure 9. The micrometer is clamped onto the outer surface of the pipe using a collar. Different types of adaptors were made to accommodate the various kinds of probes used in this study.

The relative position of the hot-film probes to the inner surface of the pipe can be established using a micrometer once the thickness of the pipe is known. The air gauge technique, described in Section 4.1.1 is then applied to fine tune the flushness. The air gauge used is locally made and is shown in Figure 10. It is described in detail in Appendix I.

4.1.1 The Air Gauge Technique

A constant air pressure is supplied to the gauge. The air jet from the gauge nozzle (see Figure 10) is brought into alignment with the calibration test hole by using a traversing mechanism with longitudinal and transverse feed. After alignment, the jet is moved slightly ahead of the test hole and the gauge pressure at the pipe wall is noted. The gauge is then realigned with the test hole. The hot-film

probe may then be lowered into the test hole and adjusted for depth by monitoring the gauge pressure. The probe is flush with the inside pipe wall when the air pressure reading at the test hole match that taken at the solid wall. To ensure that the jet is always at the same clearance away from the wall of the pipe, two adjustable pins were attached beside the jet on the pneumatic gauge. When the two prongs come into contact with the surface of the wall, a circuit between the wall surface and the prong is completed. This circuit is monitored by an ohmmeter. Thus the pin can be used as a reference point for the probe position tooling.

The constant pressure to the air gauge is supplied by a main line. This line supplies air pressure to various laboratories in the building. During the initial stage of the experiment, it was discovered that the supply pressure was very unsteady. Consequently, it was unable to maintain a constant pressure to the pneumatic gauge. To remedy the situation, a filtering tank was installed between the supply line and the air gauge to minimize the fluctuation.

4.2 Mounting of Glue-on Probe

The surface of the pipe was cleaned with fine emery paper and wiped with degreaser (M-prep neutralizer 5).

While waiting for the surface to dry, a piece of tape was carefully placed over the sensor so as to protect the sensing element when mounting. The substrate of the sensor was then covered with a layer of catalyst (200-catalyst). Before taping the sensor onto the wall surface, a thin layer of adhesive (M-bond 200) was spread over the pipe wall surface in order to aid bonding. The sensor was then placed over the pipe wall and held under finger pressure for a few minutes. The covering tape was then carefully peeled off leaving the sensor exposed. A metal plate was mounted onto the outside surface of the pipe to provide sturdy lead connections to the instrumentation.

The mounting of the glue-on type probe presented two disadvantages when compared with the flush-mounting types. Firstly, it is designed to permanently adhere to the wall of the pipe at which measurements are to be taken, thereby losing its portability. Secondly, the copper lead connections to the probe can cause disturbance in the wall boundary layer thereby resulting in erroneous measurements.

The first disadvantage was overcome by mounting the glue-on probe on a short section of steel pipe 45 cm in length. It was then carefully fit flush and butt with the

other test sections. It was thought initially that the pipe section was not long enough to eliminate the effect of the joint on measurements at the measuring stations. Hence, tests were run to investigate the effect of various joints on the flow. As shown in Figure 11, for pipe sections of identical material and diameter, no section joint effect on the pipe flow is seen. The effect of joints between those of steel and plastic pipe will be discussed in Section 5.2.

The second disadvantage was overcome by carefully drilling a small hole through the pipe to carry the electrical leads out of the pipe and soldered onto the metal plate. The hole was then sealed to prevent air leakage through the measuring station.

4.3 Temperature Sensitivity

During the calibration tests, it was discovered that the voltage output drifted with time. For a given constant shear stress loading, the corresponding voltage output always tends to decrease after a while. This could be due to the fact that the overheat ratio of the hot-film probe decreases as the stream temperature increases with time. Consequently, any decrease in the output voltage will translate into smaller measured wall shear stress values.

In order to apply the correction due to the temperature changes in the fluid, the effect of temperature changes of the fluid on the output voltage has to be determined. This can be done experimentally as was done by Kreplin and Meier (1977) by operating the hot-film probe in the wind tunnel at constant velocity over a period of time while the air is continuously warmed due to friction. Hence the hot-film probe was subjected to different temperature differences. The output voltage and the air temperature in the free stream were measured simultaneously during this period of time.

From the measurement of output voltage and the corresponding free stream temperature of the flow, correction factors for the temperature sensitivity of the various hot-film probes can be obtained from the relationship:

$$\Delta E/\Delta T = \frac{\Delta E}{\Delta t} \Big/ \frac{\Delta T}{\Delta t}$$

where E is the voltage, T the temperature and t the time interval.

Burchill and Jones (1971) proposed a scheme in which the resistance in the anenometer bridge controlling the sensor temperature is manually adjusted as the fluid

temperature changes. These adjustments are based on the calibration curves obtained earlier for different ambient temperatures. However, this scheme can be very time consuming.

4.4 Probe Calibration

Ludweig (1950) has derived the relationship between wall shearing stress and heat transfer from the film. The relationship emerges from the fact that velocity appears in the heat transfer equation as a part of the mass flow rate quantity. In the vicinity of the wall, velocity has been experimentally determined to be a function of friction velocity, i.e. $U/U^* = f\,(U^*y)/\nu$. It is the friction velocity term, U^*, which contains the shear stress quantity, such that:

$$U^* = \sqrt{\tau/\rho}$$

The heat transfer and velocity profile equations are then solved simultaneously for the heat transfer modulus, in the form of Nu, as a function of τ_w . In the case of the hot-film, Nu, and consequently τ_w , must be related to the

energy supply to Joulean heating of the probe. The resulting relationship is a 1/3 power law where:

$$E^2 = A\,\tau_w^{1/3} + B \quad \ldots\ldots (1)$$

This equation was derived assuming a laminar flow condition and was assumed to hold for turbulent flow provided that the thermal boundary layer was much thinner than the viscous sublayer. To ensure this condition, a quantitative criterion was developed such that

$$\frac{(U*l)}{\nu} < 64\ Pr$$

where l is the hot-film length, ν is the kinematic viscosity and Pr is the Prandtl number. The constant A in equation (1) consists of fluid and probe properties pertinent to heat transfer from the flow. The value of A will vary from fluid to fluid. It can also vary if the average fluid temperature changes significantly. The constant B is simply the heat flux at zero shear stress.

Hot-film calibration is required to experimentally obtain the relationship between the three variables (wall shear stress, power dissipation, and coefficient A and B) in equation (1); and to compare the actual probe behaviour with the theoretical 1/3-power equation. Having assessed the validity of the theoretical equation, an analysis fit of the calibration data can be attempted.

The hot-film probe is calibrated by subjecting it to known shear stress and noting the corresponding voltage output from the instrument. The probe is mounted well downstream of the contraction cone where the flow has been verified to be a fully developed turbulent flow. Knowing that the probe is mounted in the fully developed turbulent flow, the wall shear stress can be found from the pressure losses along the pipe using equation (7) as shown below. Note that in a fully developed turbulent pipe flow, the flow patterns are, on the average, steady as well as homogeneous, in the flow direction. The equations describing the mean motion for the flow are given by

$$\frac{1}{\rho}\frac{\partial p}{\partial x} = -\frac{1}{r}\frac{d}{dr}\left(r\,\overline{uv}\right) + \nu\,\frac{1}{r}\frac{d}{dr}\left(r\,\frac{d\bar{u}}{dr}\right) \quad \ldots\ldots (2)$$

$$\frac{1}{\rho}\frac{\partial p}{\partial r} = -\frac{1}{r}\frac{d}{dr}\left(r\,\overline{v^2}\right) + \frac{\overline{w^2}}{r} \quad \ldots\ldots (3)$$

Both of the above equations are independent of x. Therefore, P is a linear function of x and

$$\frac{\partial \bar{p}}{\partial x} = \frac{d\bar{P}_s}{dx}$$

where P_s is the mean static pressure at the wall. Equation (2) is arranged as

$$\frac{1}{r}\frac{d}{dr}\left[r\frac{\mu}{\rho}\frac{d\bar{u}}{dr} - r\overline{uv} \right] = \frac{1}{\rho}\frac{d\bar{P}_s}{dx} \quad \ldots\ldots (4)$$

multiplying equation(4) by $r\rho$ gives

$$\frac{d}{dr}\left[r\mu\frac{d\bar{u}}{dr} - r\rho\,\overline{uv} \right] = r\frac{d\bar{P}_s}{dx} \quad \ldots\ldots (5)$$

Integrating equation (5) with respect to r gives

$$r\mu\frac{d\bar{u}}{dr} - r\rho(\overline{uv}) = \frac{r^2}{2}\frac{d\bar{P}_s}{dx} + C \quad \ldots\ldots (6)$$

At C = 0

$$\mu\frac{d\bar{u}}{dr} - \rho\,\overline{uv} = \frac{r}{2}\frac{d\bar{P}_s}{dx}$$

Since $\overline{uv}=0$ at the pipe wall, it follows that at r = R, the radius of the pipe

$$\mu\frac{d\bar{u}}{dr} = \frac{R}{2}\frac{d\bar{P}_s}{dx}$$

or

$$\mu\frac{d\bar{u}}{dr} = \tau_w = \frac{R}{2}\frac{d\bar{P}_s}{dx} \quad \ldots\ldots (7)$$

The shear stress acting on the sensor in the calibration tunnel was varied by changing the mass flow rate through the pipe. The wall shear stress versus contraction cone pressure drop of Figure 12 shows the shear stress calibration curve for metal pipes.

Having calibrated the probe, a measurement of the probe operating point will determine the wall shear stress. The mean anemometer output voltage could be used directly to calculate the total anemometer bridge power dissipation. Alternatively, the actual film power loss can also be obtained as follows.

The voltage drop across the hot-film (E_f) is given by

$$E_f = \left(\frac{R_s}{(R_s + R_b + R_L)}\right) * E_b$$

where R_s is the resistance of the sensor, R_b is the bridge top resistance, R_L is the lead resistance and E_b is the anemometer output. The only effective variable resistance during operation is the sensor resistance. The film power loss is then given by

$$P_{film} = (E_f)^2/R_s$$

where P_{film} is the power loss of hot-film sensor. A functional schematic of the anemometer system is shown in Figure 13.

The probe was calibrated three times per pipe under identical conditions. Bellhouse and Schultz suggested that basing a calibration on only two points should lead to an

error of less than five percent in the measured shear stress values. In the present study, a total of about ten points were measured per run.

The selection of contraction cone pressures covered a range of shear stress up to about 0.25 mm of water. The highest contraction cone pressure utilized was 3.0 inches of water. This measurement range was selected in an attempt to avoid excessive induce vibration and pulses resulting from higher pressure differentials at the contraction cone.

At each speed increment, a reading of the output voltage and the cone pressure was taken. Immediately after each run, the pipe was rotated ninety degrees and a second calibration was performed. Afterwards, the pipe was again rotated by another ninety degrees and a third calibration was performed. The data from each calibration was evaluated by the method of least squares. The same procedure was repeated for every test pipe. The fluid temperature was monitored during the course of the experiment. A Fisher brand mercury thermometer was used and was capable of detecting temperature change of 0.1°F.

Based on the calibration from the fully developed turbulent flow, the measurements were extended into the developing flow region with the DISA-55R47 hot-film probe.

CHAPTER 5

RESULTS AND DISCUSSION

5.1 Fully Developed Turbulent Pipe Flow

The mean velocity profiles and higher-order moments were measured across the pipe diameter at two locations, namely, 78D and 98D to confirm that fully developed turbulent flow did exist.

The ratio U_b/U_c, where U_b is the bulk velocity and U_c the centreline velocity, is shown in Figure 14. The value of the ratio ranges from 0.82 - 0.83 in the Reynolds number range 0.6×10^5 to 2.30×10^5. These values are the same as those of Sabot (1976) who obtained a ratio of U_b/U_c in the range of 0.82 - 0.83 for Reynolds numbers of 5.58×10^4 to 1.12×10^5. In addition, Lawn (1971) also reported values of U_b/U_c in the range of 0.806 - 0.833 for $3.50 \times 10^4 < Re < 2.50 \times 10^5$ and L/D = 59. Comparison of the present result and those of Sabot and Lawn indicates that the present flow is fully developed.

The ratio of $U_{3/4}/U_b$, where $U_{3/4}$ is the 3/4-radius velocity, is plotted in Figure 14. In turbulent pipe flow, the 3/4-radius velocity is generally used to approximate the pipe bulk velocity. As such the $U_{3/4}/U_b$ ratio is expected to be approximately 1. The value found here for $U_{3/4}/U_b$ is

1.02. This difference may be due to not being exactly at the 3/4 radius.

The velocity profiles for Reynolds numbers of 1.14×10^5 and 2.31×10^5 at L/D = 78 and L/D = 98 are shown in Figure 15. The results indicate that the turbulent air flow in the present study is indeed fully developed in that each velocity distribution is invariant in the axial position.

Based on the law of the wall, the skin friction coefficient and the disappearance of intermittency, Patel and Head (1969) attempted to establish the minimum Reynolds number that will ensure fully developed flow. However, they were unable to establish a unique minimum Reynolds number whereby the flow can be said to be fully developed turbulent flow. In spite of that, Figures 13 and 14 and Table 1 of their paper seem to suggest that the minimum Reynolds number should be greater than 10^4. The present study has a minimum Reynolds number of $5.5. \times 10^4$, well in excess of the Patel and Head Reynolds number requirement. In addition, Figure 16 shows that the skin friction measurements, ($C_f = \tau/0.5\rho U_b^2 = 2 (U^*/U_b)^2$ are in excellent agreement with the well-known Blasius 1/4-power friction law, $C_f = 0.079 Re^{-1/4}$. Therefore, the present flow can be regarded as fully developed turbulent flow.

In the literature, some authors use the linearity of the static pressure drop along the pipe wall as a criteria for fully developed pipe flow. Although only four points are used, Figure 17 indicates that a linear relationship for the static pressure drop along the pipe wall exists.

The velocity distribution in the wall region are examined next to see if they follow the semi-logarithmic law

$$U^+ = A \ln (Y^+) + B, \quad 30 < Y^+ < 300$$

where A and B are universal constants. The mean velocity measurements in the wall region were obtained with a Pitot tube and are shown in Figure 18 as a non-dimensional plot of U^+ vs Y^+. The value of the non-dimensional position is determined from the relation $Y^+ = YU^*/\nu$ where U^* is determined from the pressure drop over the pipe length and ν is the kinematic viscosity of air. A review of the values of A and B used by different investigators can be found in Brederode and Bradshaw (1974). The non-dimensional velocity plot shows a universal region for A = 1/0.41, where 0.41 is the Karman constant, and B = 5.0 for a smooth wall. The expression can be written as $U^+ = 2.44 \ln (Y^+) + 5.0$, thus we have a usual log-law in the wall region.

The skewness factor or third order moment was examined next. Figure 19 shows the skewness factor in the longitudinal direction $S(u) = \overline{u^3}/(\overline{u^2})^{3/2}$ at L/D = 78 and 98

for two Reynolds numbers, Re = 1.14×10^5 and 2.31×10^5. The figure shows that the measured quantities are the same at both locations. Hence, the flow is, to all intents and purposes, fully developed.

Kassab (1986) used the same set-up and did the measurements at three stations one diameter apart for a Reynolds number of 1.15×10^5. A comparison of his results and those from the present study for some second - and third - order moments, $\overline{w^2}$ and $\overline{vw^2}$, are given in Azad et al (1986). Figure 20 shows the close agreement between the two sets of results.

The insensitivity to axial position of the turbulence intensity profile was checked by taking the measurements across the horizontal cross-sectional area of the pipe. The measuring stations were located at L/D = 78 and 98 for Reynolds number Re = 1.14×10^5. Figure 21 shows the results for u'/U^*, v'/U^* and w'/U^* for Re = 1.14×10^5. These were obtained using the X-wire probe. The turbulence velocities were normalized by the friction velocity calculated from the relation

$$U^* = \left[5.2749 \times \left(\frac{273 + t}{BP}\right) \times \frac{\Delta P}{\Delta(X/D)} \right]^{1/2} \quad \ldots\ (8)$$

where t is the fluid temperature in °C, BP is the measured

Barometric pressure in mm Hg, ΔP is the wall static pressure drop in mm of water along the distance x in the downstream direction, and D is the diameter of the pipe. Similar measurements were repeated for Re = 2.31×10^5 and the results shown in Figure 22. It can be seen that u'/U^* for both locations and Reynolds numbers tested are superimposed onto a single curve. A similar phenomenon was observed for v'/U^* and w'/U^*. The results clearly demonstrate that the flow is axisymmetric and there is no effect from the entry conditions at either measuring station.

Sabot and Comte-Bellot (1976) stipulate that the pipe total length, L, from the pipe inlet to the measuring station should be more than the resultant length, $L_1 + L_2$, where L_1 is the length required by the initial boundary layers to meet and L_2 is the length that ensures the renewal of turbulence. They examined this condition experimentally and stated that $L_1 = L_2 = 35D$ for their fully developed pipe flow. Their pipe diameter, D, was 10 cm and their highest Reynolds number was 1.12×10^5. A comparison of the Sabot and Comte-Bellot values and that of the present study at D = 10.16 cm and Re = 1.14×10^5 suggested that since $L_1 + L_2 > 70$, the flow for the present study is fully developed.

The results of the shear stress measurements at L/D =

78 and 98 for Reynolds number Re = 1.14×10^5 and 2.31×10^5 are presented in Figure 23. The scatter between the points was observed as the X-wire came closer to the wall. Lawn (1971) attributes this increased scatter to the deflection of the flow by the probe. The results obtained at both stations for both Reynolds numbers are identical, as shown in Figure 23, indicating fully developed turbulent flow exits.

The correlation coefficients, $\overline{uv}/u'v'$, are plotted in Figure 24. The highest correlation coefficient obtained is 0.4, and is independent of the Reynolds numbers. Figure 25 presents the distribution of $\overline{vq^2}/U_b^3$, the triple product term in the turbulent transport of turbulent energy, across the pipe diameter at L/D = 78 and 98 for Reynolds numbers of 1.14×10^5 and 2.31×10^5. The term $\overline{vq^2}$ is obtained from the relation $\overline{vq^2} = (\overline{vu^2} + \overline{v^3} + \overline{vw^2})$. The results of correlation coefficients and the $\overline{vq^2}/U_b^3$ also suggest that the fully developed turbulent flow exist.

All the above physical features of flow presented in support of fully developed flow were required for the validity of equation (2) and (3) previously quoted.

5.2 Hot-Film Probe Calibration

The three types of hot-film probes, a DISA-55A92 flush-mounted probe, a DISA-55R47 glue-on probe, and a TSI-1237 flush-mounted probe were successfully calibrated using the method described previously in Section 4.0. The calibration results are plotted using the squared output voltage, E_b^2, and the 1/3-power of the wall shear stress, τ_w, as co-ordinates. The working equation may be written in the form

$$E_b^2 = A\,\tau_w^{1/3} + B \qquad \ldots (1)$$

The resulting equations are listed on the corresponding figure for each run. The straight line equations were arrived at by a least square fit of the data points.

Two checks were made of the calibration procedure as follows. First, both the DISA-55A92 and the TSI-1237 flush-mounted probes were removed, and then later re-positioned and re-calibrated at the same station on the steel pipe. The results are presented in Figures 31 and 36 which show good repeatability. Second, the same measurement was repeated twice by rotating the pipe 90° and 180° with respect to the original position of the pipe. The calibration results for each probe tested are discussed in the following paragraph. Samples of the results for each probe are presented in Table 3 - 10 inclusive.

The calibration curves for the DISA-55R47 glue-on probe mounted onto steel pipe are shown in Figure 26. The measured points are in agreement with the 1/3-power law. The results for the three test runs on the same pipe are almost identical. They have almost the same slope and intercept.

The calibration curves for the DISA-55A92 probe flush-mounted on different metal pipes were plotted in Figures 27 to 30 inclusive. Again, the 1/3-power law is a good approximation of the measured points. The three test runs were conducted on each pipe for each probe. It can be seen that the results are essentially the same for each probe calibrated on the same pipe. A difference of less than 5% is observed. For DISA-55A92 probe, error bands for the constant A and B in equation (1) are ± 1.1 and ± 4.1 respectively.

The calibration curves for the TSI-1237 hot-film probes are plotted in Figures 32 to 35 inclusive. It has an error band of ± 1.6 for constant A and ± 2.03 for constant B of equation (1) when the results for all the pipes are considered. E_b^2 is again proportional to $\tau_w^{1/3}$. Therefore, all the probes used in this study seem to confirm that the relationship between the shear stress at the wall, τ_w, and the output voltage of the bridge, E_b, can be expressed as $E_b^2 = A\,\tau_w^{1/3} + B$.

This equation was derived from a heat balance around the sensor by assuming a laminar flow condition. The equation is also assumed to hold true for turbulent flow as long as the thermal boundary layer is much thinner than the viscous sublayer. For this requirement to be met, the following criterion must be satisfied:

$$\frac{U^* l}{\nu} < 64\ Pr \qquad \ldots\ (9)$$

For maximum and minimum tunnel operating Reynolds numbers, $Re = 1.99 \times 10^5$ and $Re = 0.59 \times 10^5$, the friction velocity, U^*, equals 1.38 ms^{-1} and 0.48 ms^{-1} respectively. Substituting values of the friction velocity, U^*, the kinematic viscosity of air, $\nu = 1.5 \times 10^{-5}\ m^2 s^{-1}$, and the DISA-55A92 probe length, $l = 0.75 \times 10^{-3}$ m, the left hand side of equation (9) yields 69.0 and 24.0 respectively.

For air, the Prandtl number is equal to 0.7 and the right hand side of equation (9) becomes 44.8. Thus, for measurements taken at Reynolds numbers greater than 1.0×10^5, the relation expressed in equation (9) has been violated. However, it is interesting to note that experimental results reveal no observable effect of the contradiction. A similar phenomenon was also observed by Coney and Simmers (1979). It is very unlikely that the linearity of calibration curves would be retained if the requirement for equation (9) has been contradicted.

Clearly, the results suggest that all the hot-film probes tested behave the same in a laminar or turbulent boundary layer. Perhaps the effect of the Prandtl number may not be that significant after all. The inequality calculations for other types of probes are presented in Table 2. The results also suggest that the dimension of DISA-55A92, TSI-1237 and DISA- 55R47 sensor element satisfy the $1 \ll Nu < Pr/C_f$ requirement.

The measured data fit the theoretical 1/3-power law very closely. This indicates that both the heat transfer analysis of the probe and the calibration techniques were correct.

Since the intercept of the calibration curves is a measure of the quantity of heat flux, the results show that the TSI-1237 hot-film probe apparently has the largest quantity of heat conducted into the substrate whereas the DISA-55R47 glue-on probe has the least. The DISA-55A92 results fall between those of the TSI-1237 and the DISA-55R47.

The results obtained for both the DISA-55A92 and TSI-1237 flush-mounted hot-film probes show that the thermal conductivity of the pipes has no appreciable effect on the calibration of hot-film probes. The shift in the

calibration curves is small and random. Comparison of Figure 32 and Figure 36, showing the calibration result of TSI-1237 flush-mounted hot-film probe mounted on steel pipe, appears to indicate that there is a small resetting or experimental error. This agrees with the observations made earlier in the positioning of the hot-film probe that the constant supply pressure from the main line to the air gauge is somewhat unsteady.

The calibration was originally to include some non-metallic pipes, namely, PVC and acrylic plexiglass pipes, so that a more complete picture of the effects of the different heat conductivity material could be examined. However, it was found that the inside diameter of both non-metallic pipes was different from the steel pipe they were to mate. As a result, attempts to fit the plastic pipe to the steel pipe sections, tight and butt, met with little success. In addition, the plastic pipes could not withstand the stresses applied to them without deforming. The special collars and pipe and machining to fit the plastic pipe to the steel section did not solve the problem of air leaking from the joint (See Figure 11). In addition, the inner wall of the acrylic plexiglass pipe was rather rough, unlike the smooth walls of the metal pipes.

Attempts were made to measure the shear stress along

the pipe in the developing flow region using the calibration curve obtained from the fully developed turbulent flow. Here the DISA-55R47 glue-on probe was used and the pipe length was systematically reduced after each measurement. The results are presented in Figure 37 for the various Reynolds numbers tested. Figure 38 shows the distribution of skin friction along the pipe length.

The results indicate that the hydrodynamic entry length is very short. Barbin and Jones (1963) have shown experimentally that the wall shear stress and the static pressure gradient attain their fully developed values within the first fifteen diameters. Their measurements were carried out at Reynolds number of 3.88×10^5, based on pipe diameter and mean velocity.

CHAPTER 6

CONCLUSIONS

This research reveals the following conclusions:

1. For Reynolds numbers in the range $1.14 \times 10^5 < Re < 2.31 \times 10^5$, the measurements of mean velocity profiles, skin friction, and various moments demonstrate clearly that the flow in the pipe is fully developed after 78 diameters of the pipe.

2. The hot-film probe can be calibrated accurately in fully developed turbulent pipe flow provided it is carefully mounted and temperature drift in the flow is accounted for.

3. The calibration confirms the usual probe response law, that the relationship between the shear stress at the wall, τ_w, and the output voltage of the hot-film bridge system, E_b, can be expressed as

$$E_b^2 = A\tau_w^{1/3} + B$$

as demonstrated by other researchers before.

4. No change of calibration curves is apparent when the flush-mounted hot-film probes are mounted on pipes of

different materials having different thermal conductivity.

5. The TSI-1237 flush-mounted hot-film probe has the highest conduction heat loss and DISA-55R47 glue-on probe the least. DISA-55A92 flush-mounted hot-film probe seems to fall in between the two.

6. The wall shear stress reaches its fully developed values in an inlet length of approximately twenty diameters.

CHAPTER 7

RECOMMENDATIONS

1. Further studies need to be undertaken to include the non-metallic pipes.

2. Similar studies should be carried out, by measuring the wall temperature precisely and simultaneously monitor the temperature of the flow, to give a more complete picture of the thermal leakage to the substrate of the various sensors. In addition, it would be interesting to explore the possibility of using two points to fix the calibration curve (Bellhouse and Schultz) in the present setting as compared to the elaborate temperature compensation scheme.

REFERENCES

1. Azad, R.S. and Hummel, R.H., 1971, "Measurement of the Intermittency Factor in Diffuser Flow", Canadian Journal of Physics, No. 23, Vol. 49.

2. Azad, R.S., Kassab, S.Z. and Dang, T.H., 1986, "Experimental Evaluation of Approximations for w^2 and vw^2", AIAA Journal (to be published).

3. Azad, R.S., Kassab, S.Z. and Dang, T.H., 1985, "Experimental Evaluation of Approximation for Moments of Fluctuating Turbulent Velocity, Namely, w^2 and vw^2", Report METR-10, Mechanical Engineering Dept., The University of Manitoba.

4. Barbin, A.R. and Jones, J.B., 1963, "Turbulent Flow in the Inlet Region of a Smooth Pipe", Transactions of the ASME, Vol. 85, Series D, pp. 29-34.

5. Bellhouse, B.J. and Schultz, D.L., 1966, "Determination of Mean and Dynamic Skin Friction Separation and Transition in Low Speed Flow with a Thin Film Heated Element", J. Fluid Mach., Vol. 24, Part 2, pp. 379-400.

6. Brederode, V. de and Bradshaw, P., 1974, "A Note on the Empirical Constants Appearing in the Logarithmic Law for Turbulent Wall Flows", I.C. Aero Rep., 74-03.

7. Brown, G.L., 1967, "Theory and Application of Heated Films for Skin Friction Measurements", Proceedings of 1967 Heat Transfer and Fluid Mechanics Institute.

8. Burchill, W.E. and Jones, B.G., 1971, "Interpretation of Hot Film Anemometer Response", Proceedings Second Symposium on Turbulence Measurements in Liquids, Rolla, Missouri.

9. Burhannauddin, S., 1980, "Measurement of Wall Shear Stress with Hot Wire Anemometer", M.Sc. Thesis, University of Manitoba.

10. Coney, J.E.R. and Simmers, D.A., May 1979, "The Determination of Shear Stress in Fully Developed Laminar Aerial Flow and Taylor Vortex Flow, using a Flush-Mounted Hot Film Probe", DISA Information No. 24.

11. Deissler, R.G., 1955, "Turbulent Heat Transfer and Friction in the Entrance Region of Smooth Passages", Transactions of the ASME, Vol. 77, pp. 1221-1233.

12. Dewey, C.F.,Jr., Huber, P.W., 1982, "Measurement Methods for Fluid Shear Stress", Annual Summary Report, Department of Mechanical Engineering, Massachusetts Institute of Technology.

13. Fage, A. and Falkner, V.M., 1930, Pro. Roy Soc. A129, 378.

14. Franklin, R.E. and Wallace, J.M., 1970, "Absolute Measurements of Static-Hole Error Using Flush Transducers", J. Fluid Mach., Vol. 42, Part 1, pp. 33-48.

15. Geremia, J.O., 1970, "An Experimental Investigation of Turbulence Effects at the Solid Boundary Using Flush-Mounted Hot Film Sensors", Ph.D Thesis, George Washington University.

16. Holman, J.P., "Heat Transfer", 4th Edition, 1976, McGraw-Hill Kogakwsha Ltd.

17. Houdeville, R., Juillen, J.C. and Cousteix, J., 1983, "Skin Friction Measurements with Hot-Element Gages", Paper presented before the 20th Collogue d'Aerodynamique Appliquee (AAAF) in Toulouse, November 8-10.

18. Hussain, A.K.M.F. and Reynolds, W.C., Dec. 1975, "Measurements in Fully Developed Turbulent Channel Flow", Transactions of the ASME, Vol. 97.

19. Kalumuck, Kenneth M., 1983, "A Theory for the Performance of Hot-Film Shear Stress Probes", Ph.D Thesis, Massachusetts Institute of Technology.

20. Kassab, S.Z., 1986, "Turbulence Structure in Axisymmetric Wall-Bounded Shear Flow", Ph.D Thesis, University of Manitoba.

21. Kreplin, H.P. and Meier, H.U., July, 1977, "Application of Heated Element Techniques for the Measurement of the Wall Shear Stress in Three-Dimensional Boundary Layers", EUROMECH 90.

22. Lawn, C.J., 1971, "The Determination of the Rate of Dissipation in Turbulent Pipe Flow", J. Fluid Mech., Vol. 48, Part 3, pp. 477-505.

23. Liepmann, H.W. and Skinner, G.T., 1954, "Shearing Stress Measurements by Use of a Heated Element", NACA TM3268.

24. Ludwieg, H., 1950, "Instrument for Measuring the Wall Shearing Stress of Turbulent Boundary Layers", NACA TM1284.

25. Ludwieg, H. and Tillmann, W., 1950, "Investigations of the Wall Shearing Stress in Turbulent Boundary Layers", NACA TM1285.

26. Morris, W. Rubesin, Arthur F. Okuno, George G. Mateer and Aviel Brosh, 1975, "Flush-Mounted Hot Wire Gage for Skin Friction and Separation Detection Measurements", ICIASF Record.

27. Pardo, Don Frederick, 1980, "The Influence of Substrate Conduction in Hot-Film Shear Stress Measurements", M.Sc. Theis, Massachusetts Institute of Technology.

28. Patel, V.C. and Head, M.R., 1969, "Some Observations on Skin Friction and Velocity Profiles in Fully Developed Pipe and Channel Flows", J. Fluid Mechanics, Vol. 38, Part 1, pp. 181 - 201.

29. Pessoni, D.H., 1974, "An Experiemental Investigation into the Effects of Wall Heat Flux on the Turbulence Structure of Developing Boundary Layers at Moderately High Reynolds Numbers", Ph.D. Thesis, University of Illinois, Urbana.

30. Preston, J.H., 1950, "The Three-Quarter Radius Pitot-Tube Flow Meter", The Engineer 190, pp. 400-402.

31. Rainey, F.G., 1975, "Hydraulic of Flow in a Rill", Ph.D Thesis, Purdue University.

32. Reichert, J.K., 1973, "Wall Shear Stress in Developing Turbulent Pipe Flow", M.Sc. Thesis, University of Manitoba.

33. Sabot, J. and Comte-Bellot, G., 1976, "Intermittency of Coherent Structures in the Core Region of Fully Developed Turbulent Pipe Flow", J. Fluid Mech., 74, pp. 767-796.

34. Schultz-Grunow, F., 1941, "Neues Reibungswiderstand-gesetz fur glatte platten", Luftfahrtforschung. Available as NACA TM986.

APPENDIX I

AIR GAUGE DESIGN

The air gauge used in the alignment of the hot film probe is shown in Figure 10. Air is supplied at a constant pressure of 50 psi. The flow through d_1 and through d_2 is governed by the separation distance x between the outlet and the wall of the pipe. Thus, measurement of this pressure may be taken as an indication of the separation distance x. For the purpose of this study, diameter d_1 is set at 0.3 mm and d_2 at 0.6 mm. This will give a displacement range of 0.015 mm to 0.053 mm.

PIPE MATERIAL		PIPE SECTION LENGLTH	THERMAL CONDUCTIVITY	
Commercial Name	Chemical Composition	(cm)	(kcal/hmk)	$\Lambda = \lambda / \lambda_f$
PVC		183	0.104 - 0.149	4.7 - 6.7
Acrylic Plexiglass Material		307	0.161	7.3
Steel 1020	0.23 C 0.64 Mn	400	44.63	2028
Red Brass	85 Cu	367	52	2363
Alcan Aluminum 6351-T6	1.0 Si 0.6 Mg 0.6 Mn 97.8 AL	580	183.6	8,345
Deoxidized Copper	0.005 - 0.012 P rem. Cu	366	50	2273

* λ_f is the thermal conductivity of a fluid in kcal/hmk

TABLE 1: Different Types of Pipe Used in the Calibration of Hot Film Probes

SENSOR	$Re=U_bD/\nu$	U^* (ms^{-1})	$\frac{U^*1}{\nu}$	64 Pr
TS1-1237	0.59×10^5	0.48	32	44.8
	1.99×10^5	1.38	92	44.8
DISA-55A92	0.59×10^5	0.48	24	44.8
	1.99×10^5	1.38	69	44.8
DISA-55R47	0.59×10^5	0.48	28.8	44.8
	1.99×10^5	1.38	82.8	44.8

TABLE 2: Calculation of $\frac{U^*1}{\nu}$ versus 64 Pr for Various Probes

Pipe Material = Steel
Sensor = DISA-55R47
Room Temperature = 24°C
R_h = 23.08 Ω

$$R_h = R + K_{20}R_{20}(T_s - T_o)$$

T (°F)	E_b^2 $(v)^2$	$\tau^{1/3}$ $(Nm^{-2})^{1/3}$
76.25	29.18	0.64
76.30	29.46	0.78
76.50	29.61	0.84
76.85	29.85	0.93
77.35	30.09	1.04
77.95	30.26	1.09
78.60	30.43	1.16
79.30	30.59	1.21

Table 3: Hot-Film Calibration Data for DISA-55R47 Mounted on Steel Pipe

R_h = Probe hot resistance

R = Probe resistance at 20°C

K_{20} = Temperature coefficient of sensor resistance at 20°C

R_{20} = Sensor resistance at 20°C

T_s = Selected sensor operating temperature

T_o = Ambient temperature (temperature of medium)

Pipe Material = Aluminium
Sensor = DISA-55A92
Room Temperature = 24°C
R_h = 15.67 Ω

$$R_h = R + K_{20}R_{20}(T_s - T_o)$$

T (°F)	E_b^2 $(v)^2$	$\tau^{1/3}$ $(Nm^{-2})^{1/3}$
78.85	37.22	0.67
78.60	37.95	0.80
78.50	38.27	0.87
78.55	38.59	0.94
78.80	38.91	1.00
79.20	39.29	1.07
79.70	39.63	1.14
80.20	39.87	1.19
80.80	40.12	1.23

Table 4: Hot-Film Calibration Data for DISA-55A92 Mounted on Aluminium Pipe

R_h = Probe hot resistance

R = Probe resistance at 20°C

K_{20} = Temperature coefficient of sensor resistance at 20°C

R_{20} = Sensor resistance at 20°C

T_s = Selected sensor operating temperature

T_o = Ambient temperature (temperature of medium)

Pipe Material = Red Brass
Sensor = DISA-55A92
Room Temperature = 24°C
R_h = 15.64 Ω

$$R_h = R + K_{20}R_{20}(T_s - T_o)$$

T (°F)	E_b^2 $(v)^2$	$\tau^{1/3}$ $(Nm^{-2})^{1/3}$
76.25	38.71	0.64
76.25	39.47	0.80
76.25	39.77	0.86
76.45	40.10	0.93
76.85	40.45	1.00
77.25	40.70	1.05
77.65	40.90	1.10
78.15	41.18	1.16
78.70	41.37	1.19
79.55	41.58	1.23

Table 5: Hot-Film Calibration Data for DISA-55A92 Mounted on Red Brass Pipe

R_h = Probe hot resistance

R = Probe resistance at 20°C

K_{20} = Temperature coefficient of sensor resistance at 20°C

R_{20} = Sensor resistance at 20°C

T_s = Selected sensor operating temperature

T_o = Ambient temperature (temperature of medium)

Pipe Material = Copper
Sensor = DISA-55A92
Room Temperature = 23°C
R_h = 15.54 Ω

$R_h = R + K_{20}R_{20}(T_s - T_o)$

T (°F)	E_b^2 $(v)^2$	$\tau^{1/3}$ $(Nm^{-2})^{1/3}$
74.00	38.60	0.63
74.05	39.04	0.72
74.20	39.33	0.78
74.40	39.72	0.86
74.70	40.05	0.91
75.10	40.28	0.97
75.60	40.62	1.03
76.40	40.95	1.10
76.95	41.22	1.16
77.50	41.44	1.20
78.10	41.68	1.24
78.70	41.86	1.29
79.20	42.02	1.31

Table 6: Hot-Film Calibration Data for DISA-55A92 Mounted on Copper Pipe

R_h = Probe hot resistance

R = Probe resistance at 20°C

K_{20} = Temperature coefficient of sensor resistance at 20°C

R_{20} = Sensor resistance at 20°C

T_s = Selected sensor operating temperature

T_o = Ambient temperature (temperature of medium)

Pipe Material = Red Brass
Sensor = TSI-1237
Room Temperature = 25°C
R_h = 6.42 Ω

$$R_h = R + K_{20}R_{20}(T_s - T_o)$$

T (°F)	E_b^2 $(v)^2$	$\tau^{1/3}$ $(Nm^{-2})^{1/3}$
76.60	216.96	0.64
76.85	218.97	0.76
77.25	220.39	0.84
77.85	222.08	0.94
78.50	223.27	0.99
79.25	224.29	1.06
79.90	225.25	1.12
80.55	226.15	1.16
81.35	226.68	1.19
82.00	227.64	1.25

Table 7: Hot-Film Calibration Data for TSI-1237 Mounted on Red Brass Pipe

R_h = Probe hot resistance

R = Probe resistance at 20°C

K_{20} = Temperature coefficient of sensor resistance at 20°C

R_{20} = Sensor resistance at 20°C

T_s = Selected sensor operating temperature

T_o = Ambient temperature (temperature of medium)

Pipe Material = Aluminium
Sensor = TSI-1237
Room Temperature = 23°C
R_h = 6.42 Ω

$$R_h = R + K_{20}R_{20}(T_s - T_o)$$

T (°F)	E_b^2 $(v)^2$	$\tau^{1/3}$ $(Nm^{-2})^{1/3}$
73.70	215.50	0.75
74.00	217.65	0.86
74.40	219.64	0.94
74.80	220.10	1.00
75.50	221.51	1.08
76.00	222.75	1.15
76.75	223.25	1.19
77.50	224.30	1.23

Table 8: Hot-Film Calibration Data for TSI-1237 Mounted on Aluminium Pipe

R_h = Probe hot resistance

R = Probe resistance at 20°C

K_{20} = Temperature coefficient of sensor resistance at 20°C

R_{20} = Sensor resistance at 20°C

T_s = Selected sensor operating temperature

T_o = Ambient temperature (temperature of medium)

Pipe Material = Steel
Sensor = TSI-1237
Room Temperature = 22.2°C
R_h = 6.42 Ω

$$R_h = R + K_{20}R_{20}(T_s - T_o)$$

T (°F)	E_b^2 $(v)^2$	$\tau^{1/3}$ $(Nm^{-2})^{1/3}$
73.25	232.29	0.63
73.65	234.76	0.78
74.00	236.29	0.87
74.40	237.48	0.93
74.75	238.40	0.99
75.15	239.54	1.05
75.55	240.19	1.09
76.00	241.12	1.14
76.35	241.86	1.18
76.60	242.72	1.23
76.75	243.44	1.26

Table 9: Hot-Film Calibration Data for TSI-1237 Mounted on Steel Pipe

R_h = Probe hot resistance

R = Probe resistance at 20°C

K_{20} = Temperature coefficient of sensor resistance at 20°C

R_{20} = Sensor resistance at 20°C

T_s = Selected sensor operating temperature

T_o = Ambient temperature (temperature of medium)

Pipe Material = Copper
Sensor = TSI-1237
Room Temperature = 23°C
R_h = 6.42 Ω

$$R_h = R + K_{20}R_{20}(T_s - T_o)$$

T (°F)	E_b^2 $(v)^2$	$\tau^{1/3}$ $(Nm^{-2})^{1/3}$
75.90	216.90	0.64
75.95	219.24	0.77
76.10	220.89	0.86
76.40	222.29	0.93
76.85	223.63	1.00
77.30	224.55	1.05
77.75	225.29	1.10
78.35	226.32	1.15
79.00	227.15	1.19
79.55	227.85	1.23

Table 10: Hot-Film Calibration Data for TSI-1237 Mounted on Copper Pipe

R_h = Probe hot resistance

R = Probe resistance at 20°C

K_{20} = Temperature coefficient of sensor resistance at 20°C

R_{20} = Sensor resistance at 20°C

T_s = Selected sensor operating temperature

T_o = Ambient temperature (temperature of medium)

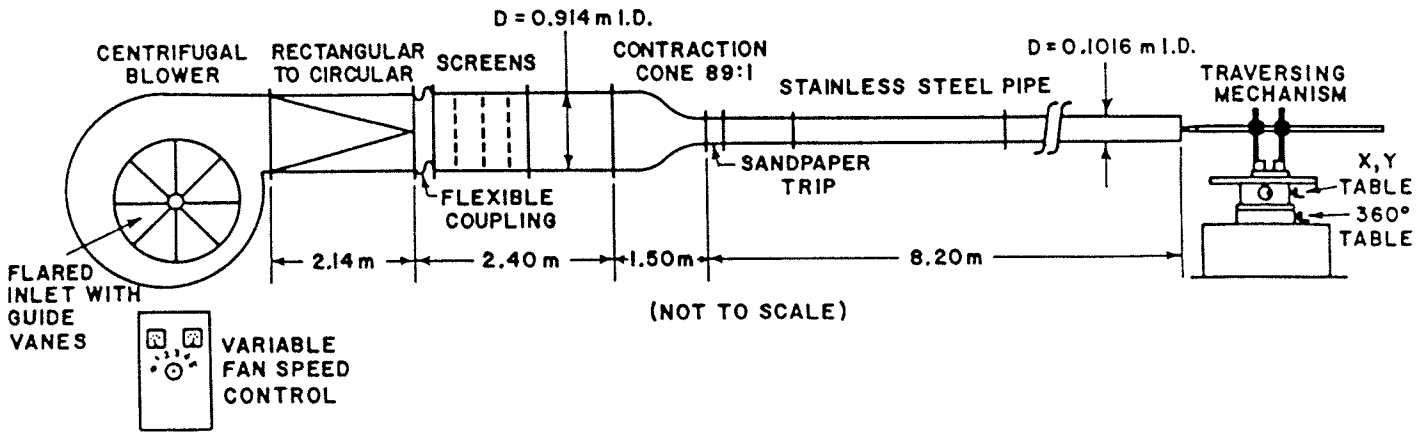

Figure 1. Layout of wind tunnel

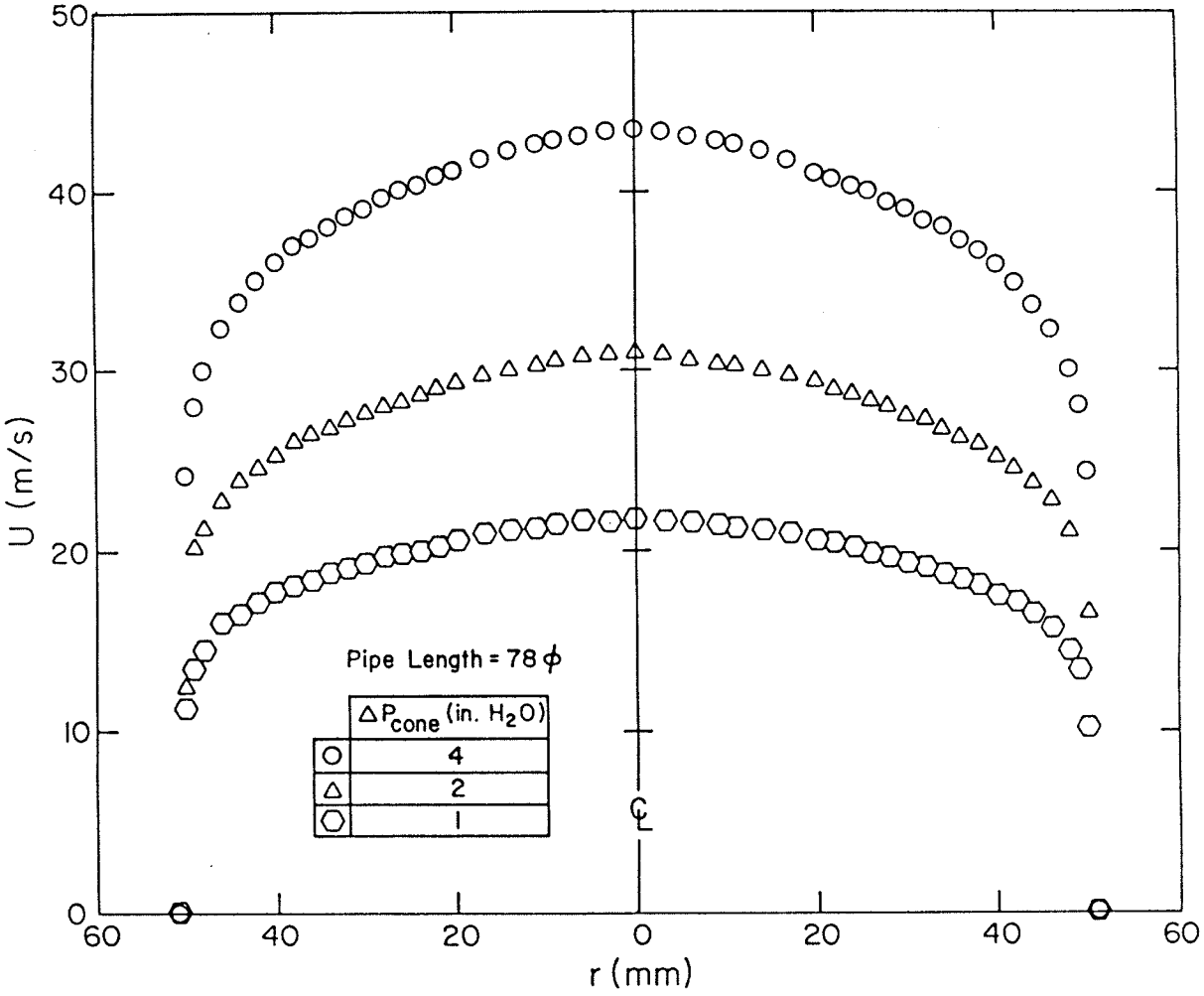

Figure 2. Velocity profile before the installation of flexible coupling

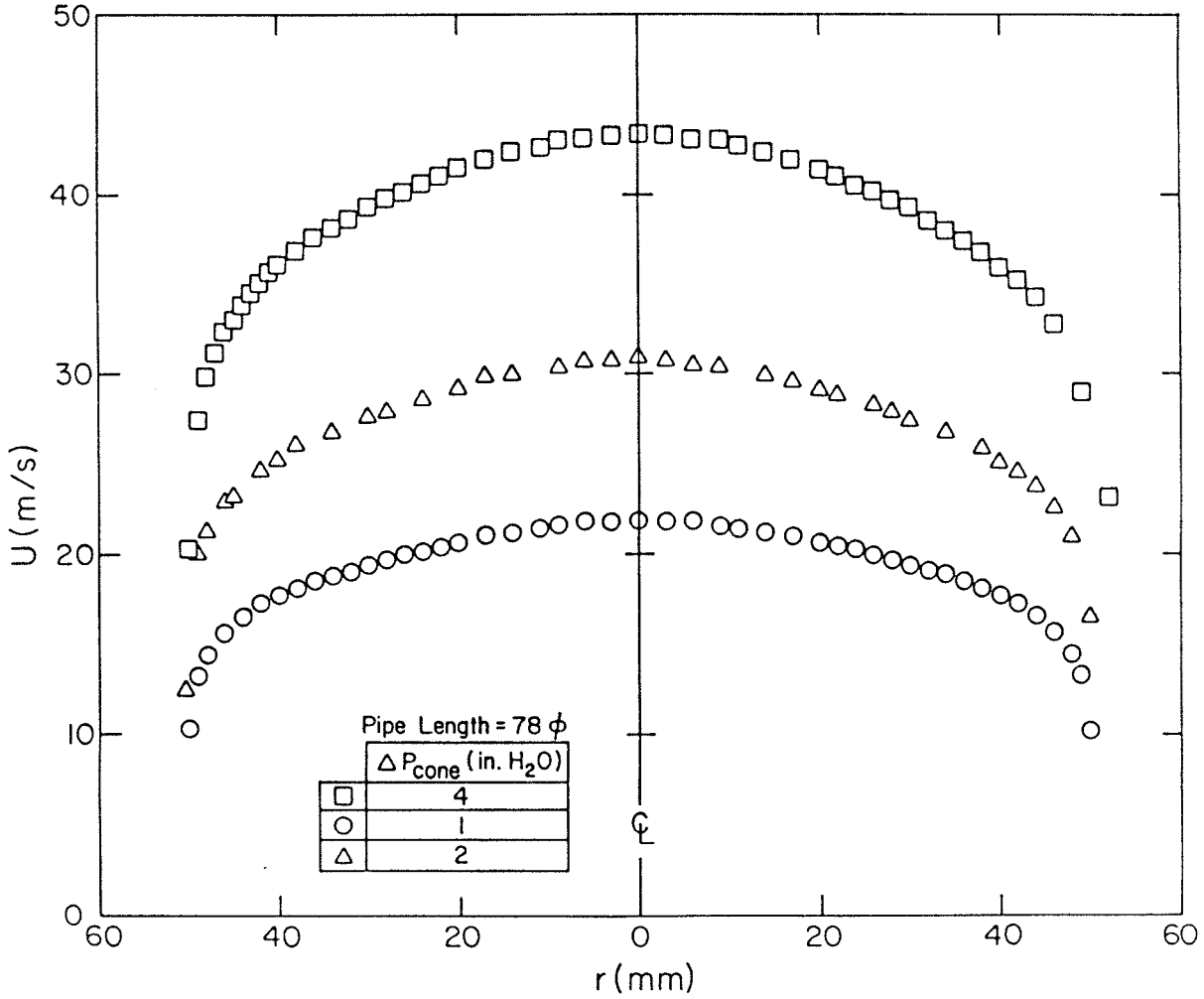

Figure 3. Velocity profile after the installation of flexible coupling

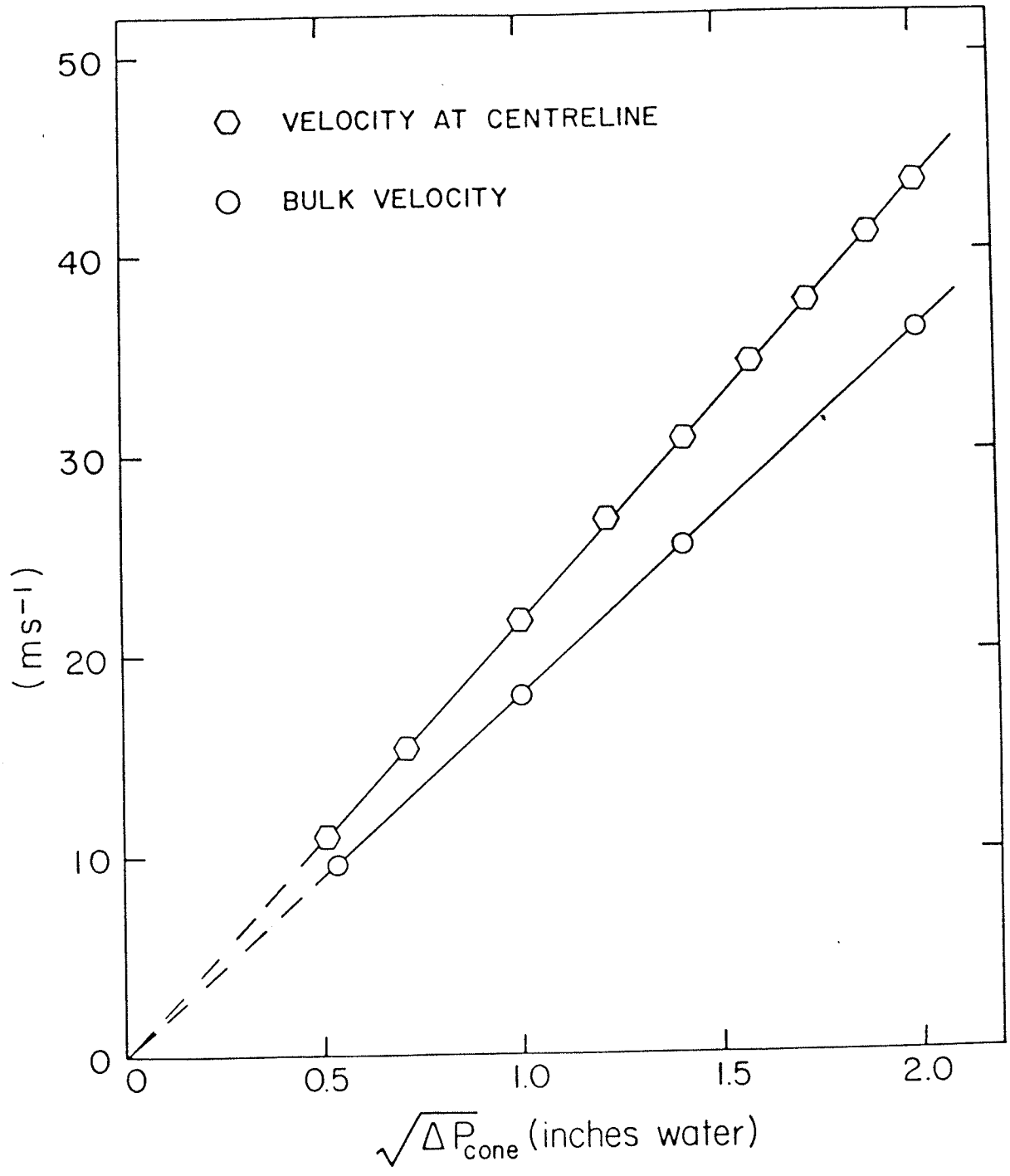

Figure 4. Wind tunnel calibration plot

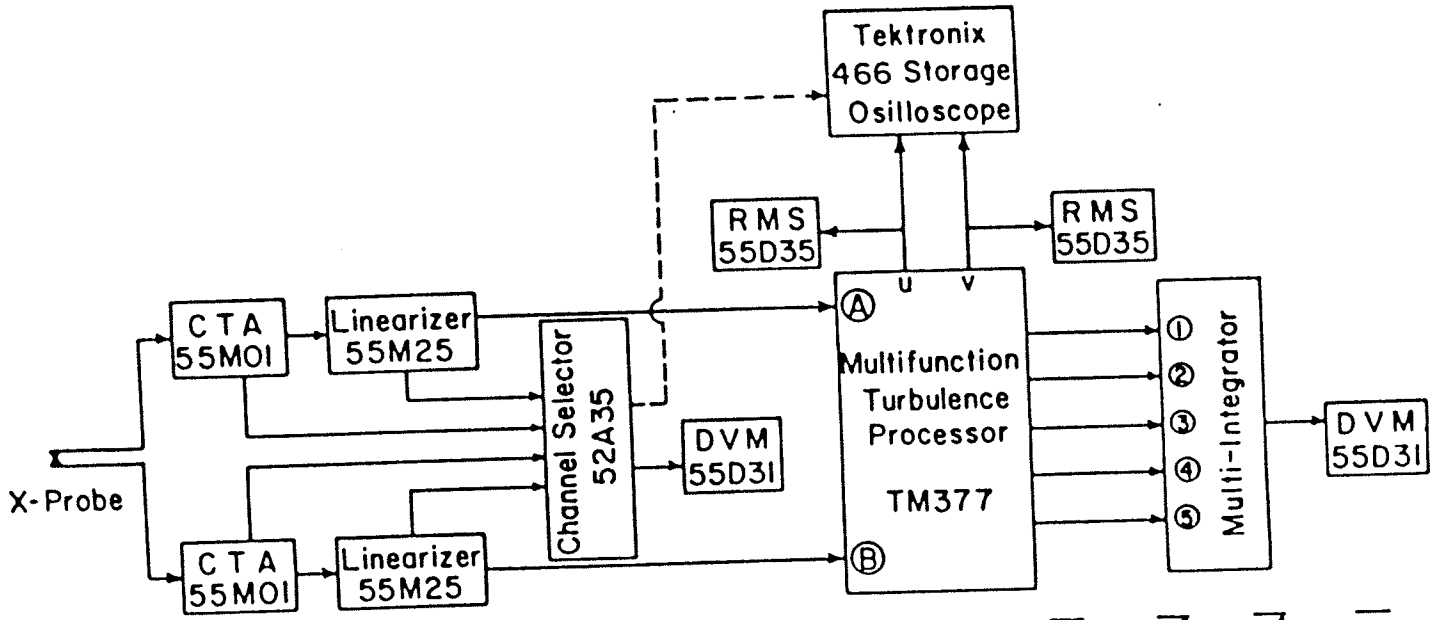

CTA Constant Temperature Anemometer

RMS Root Mean Square

DVM Digital Voltmeter

① $\frac{\overline{u^2}}{10}$, $\frac{\overline{u^3}}{100}$, $\frac{\overline{u^4}}{1000}$, $\frac{\overline{uv}}{10}$

② $\frac{\overline{v^2}}{10}$ $\frac{\overline{v^3}}{100}$ $\frac{\overline{v^4}}{1000}$ $\frac{\overline{uv^2}}{100}$

③ $\frac{\overline{uv^3}}{1000}$, $\frac{\overline{u^3v}}{1000}$, $\frac{\overline{u^2v^2}}{1000}$, $\frac{\overline{u^2v}}{100}$

④ U

⑤ V

Figure 5. Hot-wire data acquisition system

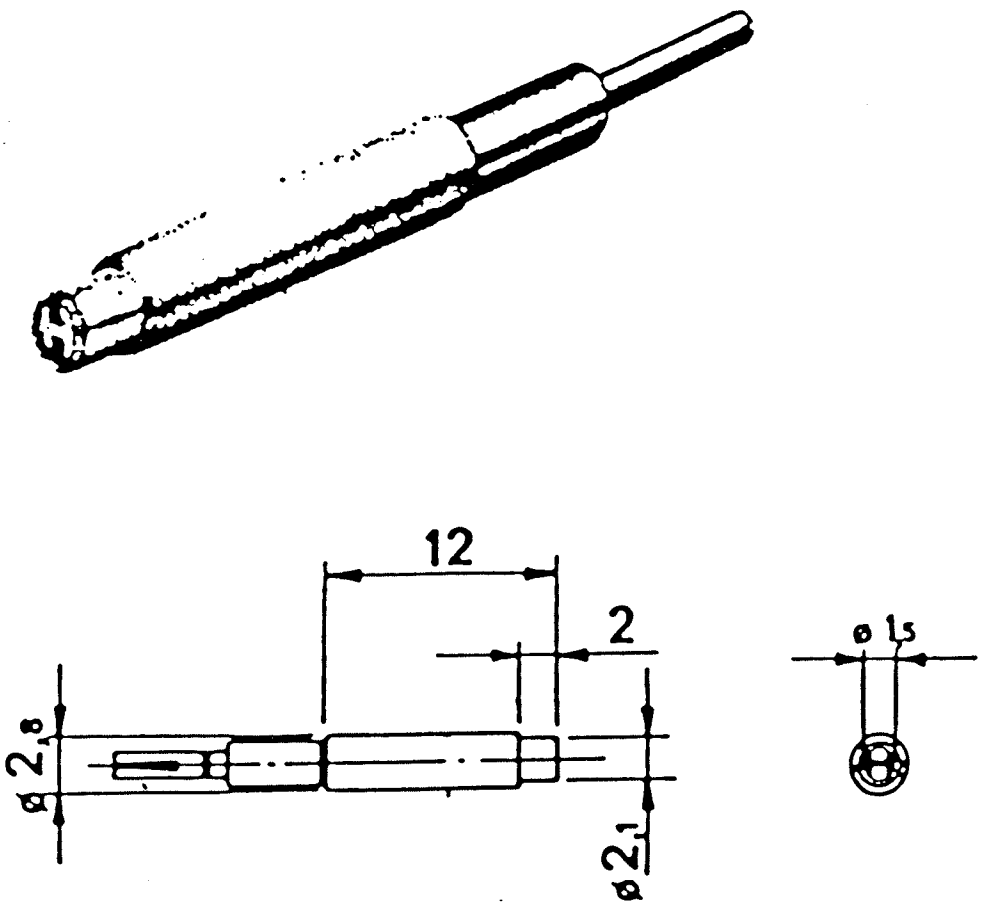

Figure 6. DISA subminiature flush-mounted hot-film probe (DISA-55A92)

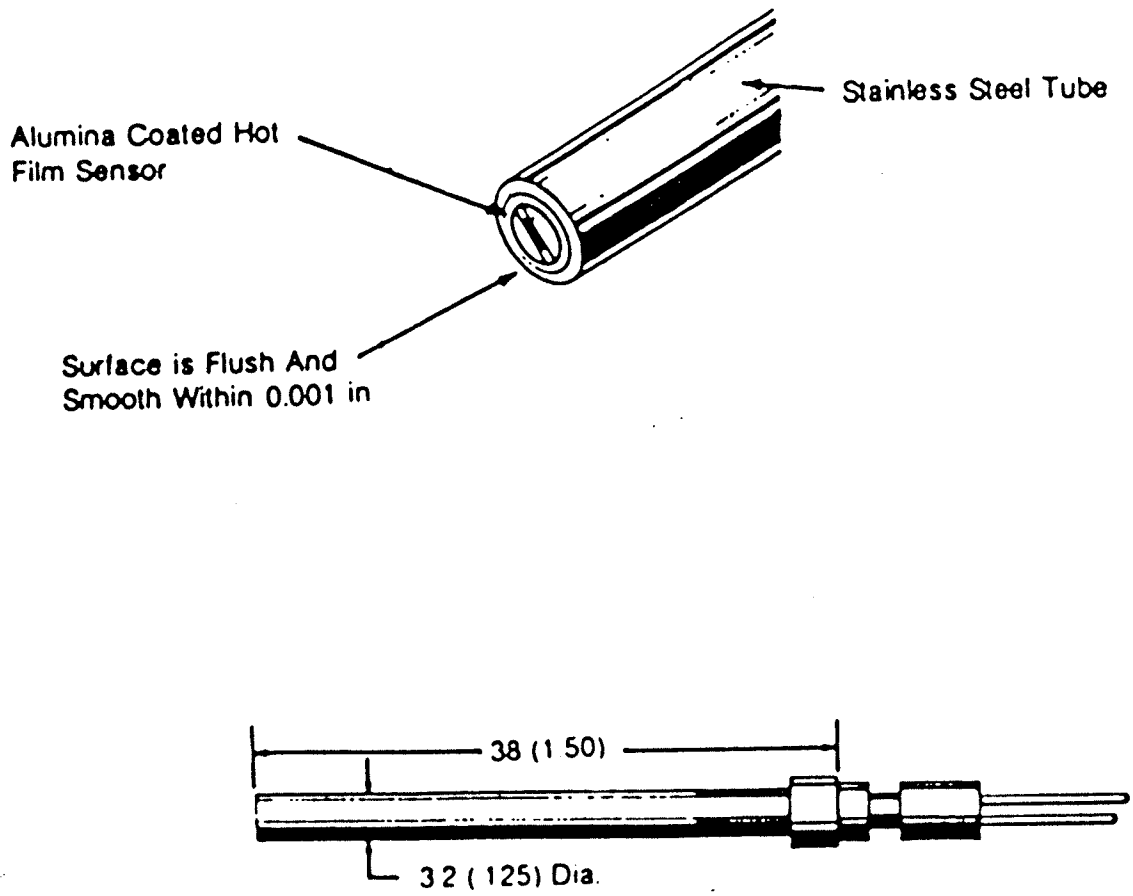

Figure 7. Thermo system flush-mounted hot-film probe (TSI-1237)

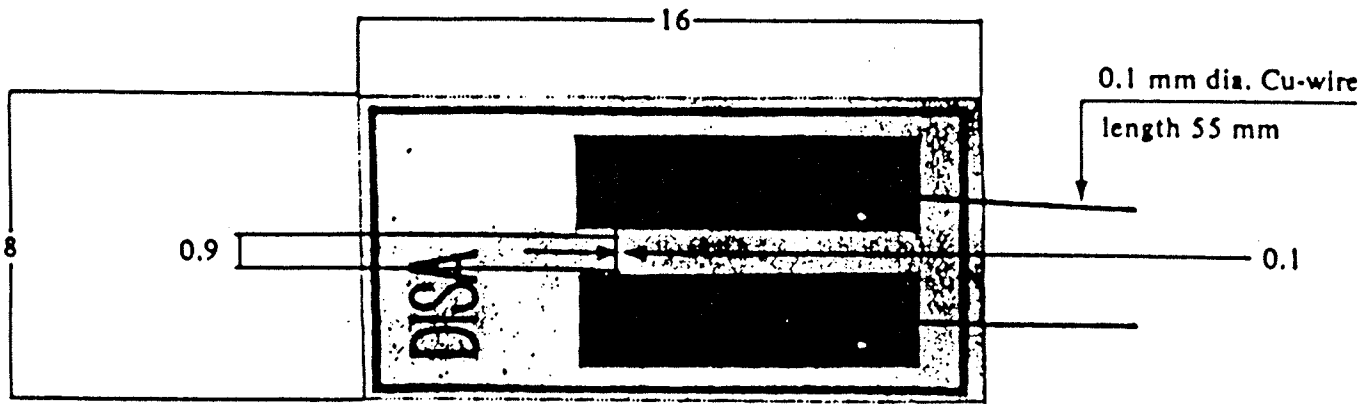

Figure 8. DISA glue-on probe (DISA-55R47)

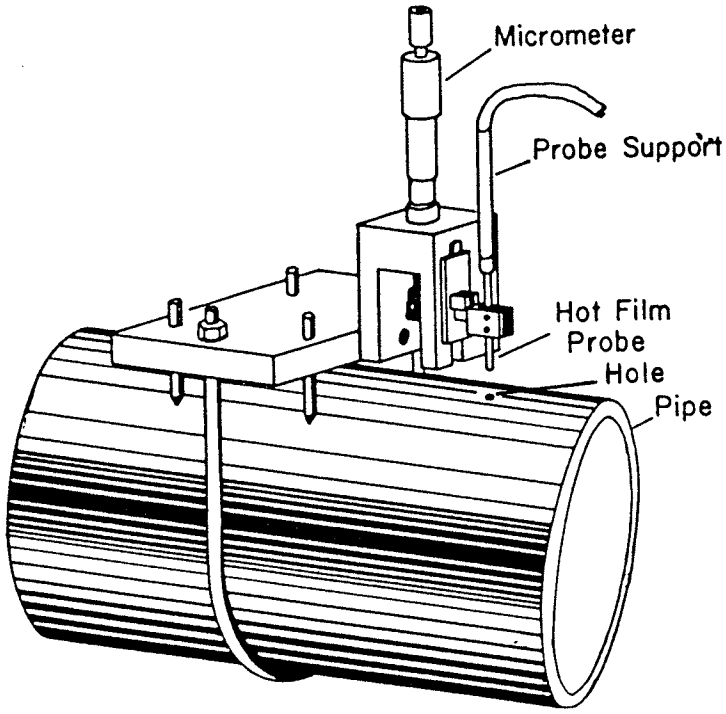

Figure 9. Hot-film probe support

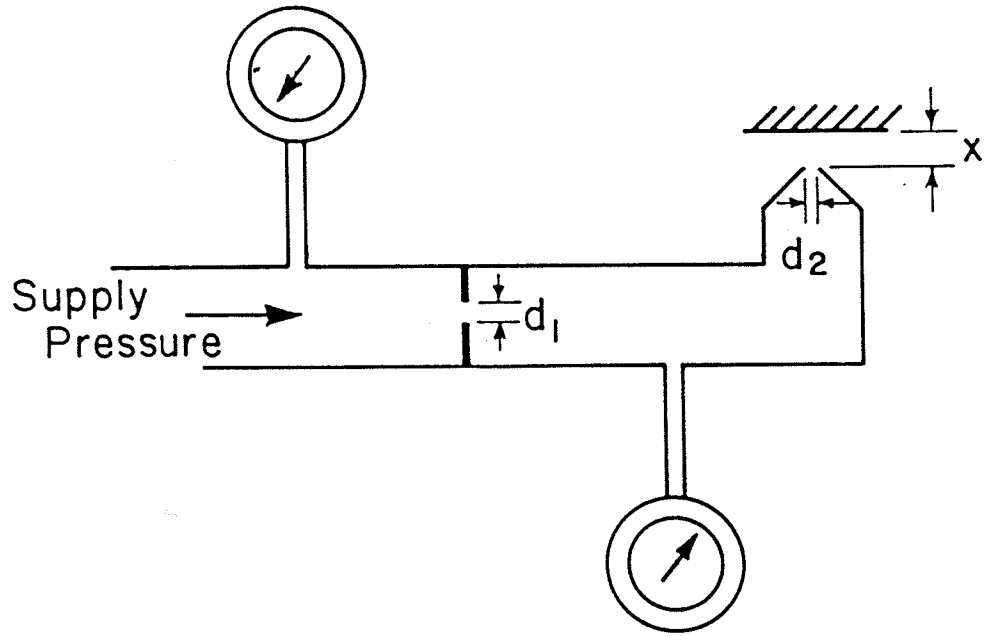

Figure 10. Air gauge design

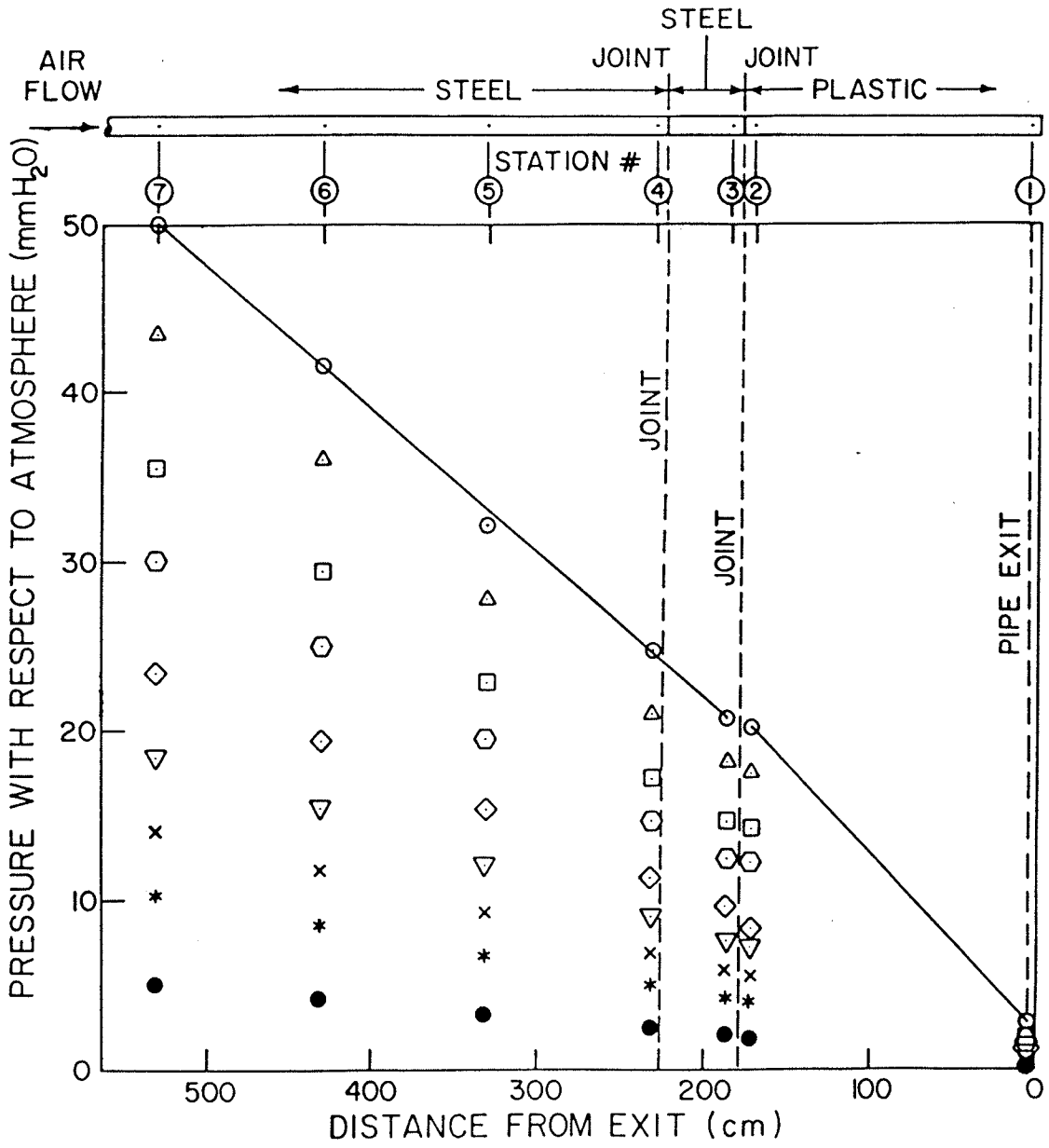

Figure 11. Effects of metal-metal and metal-plastic joints

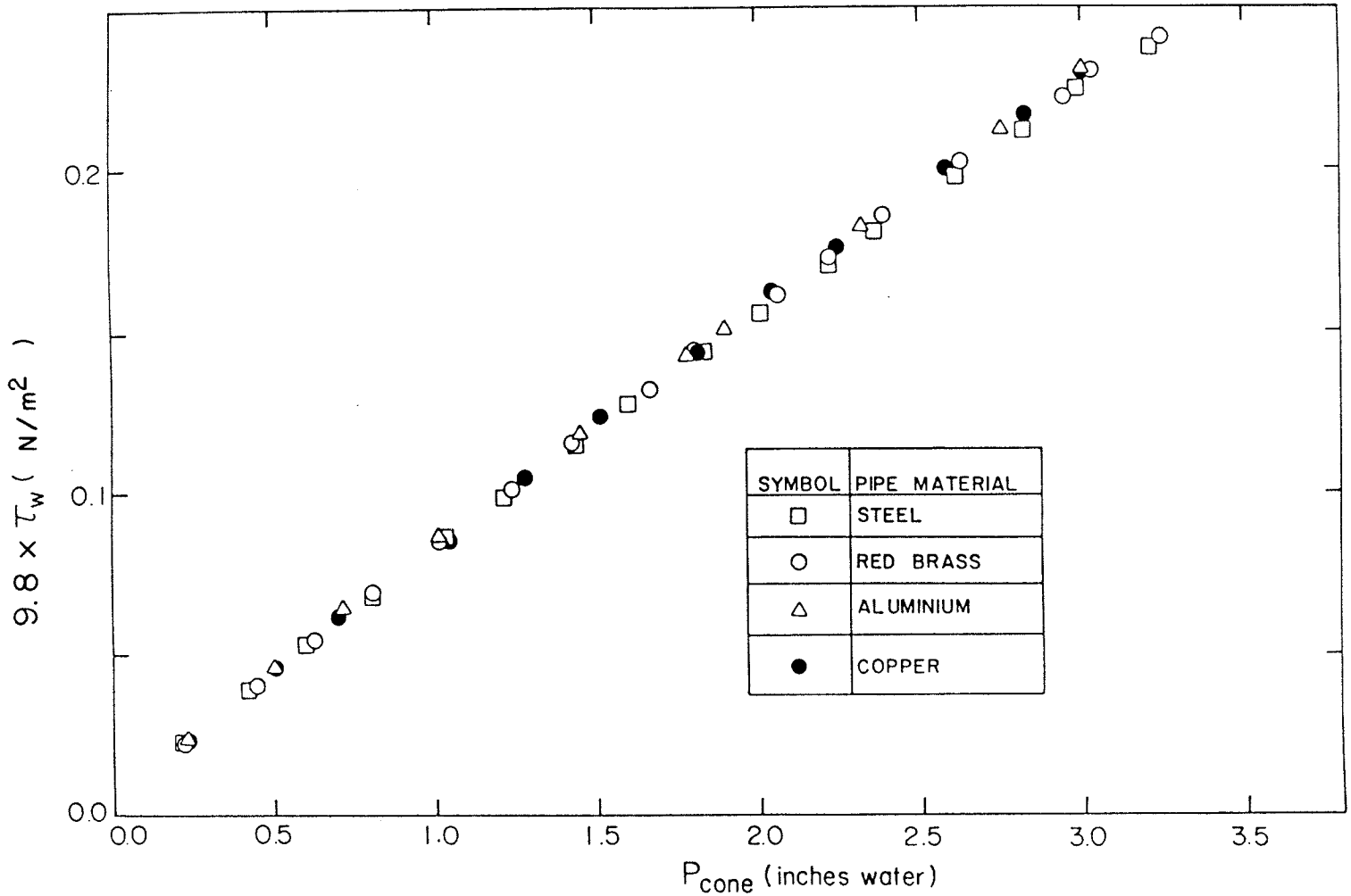

Figure 12. Shear stress calibration curve for metal pipes

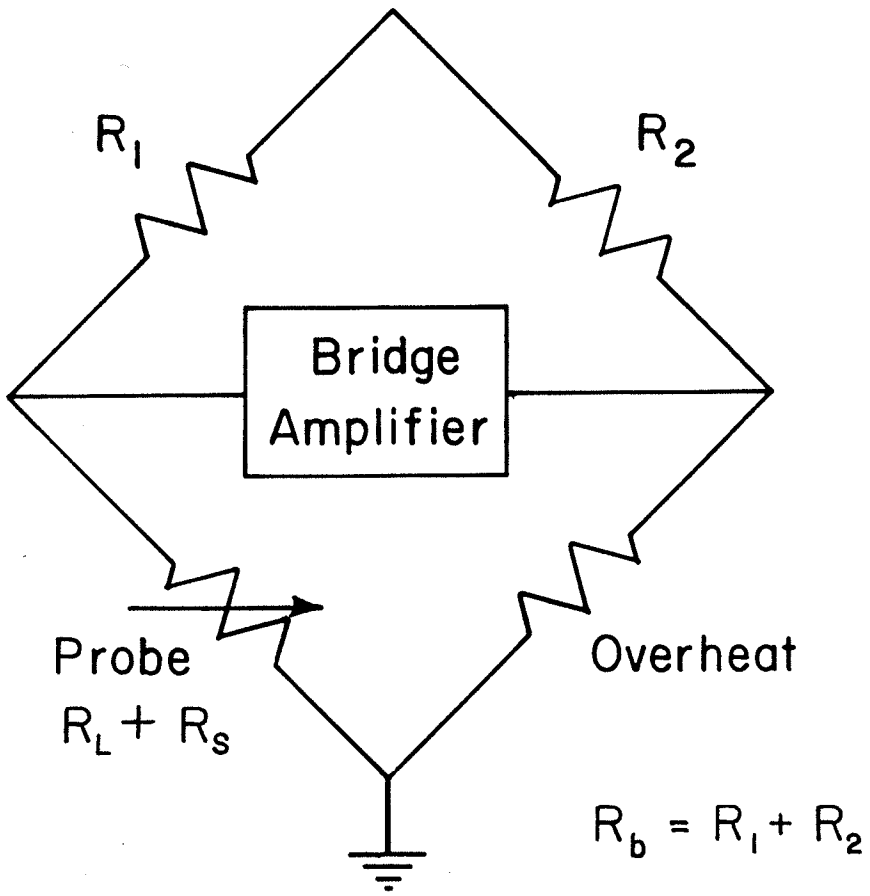

Figure 13. Hot-film sensor circuit

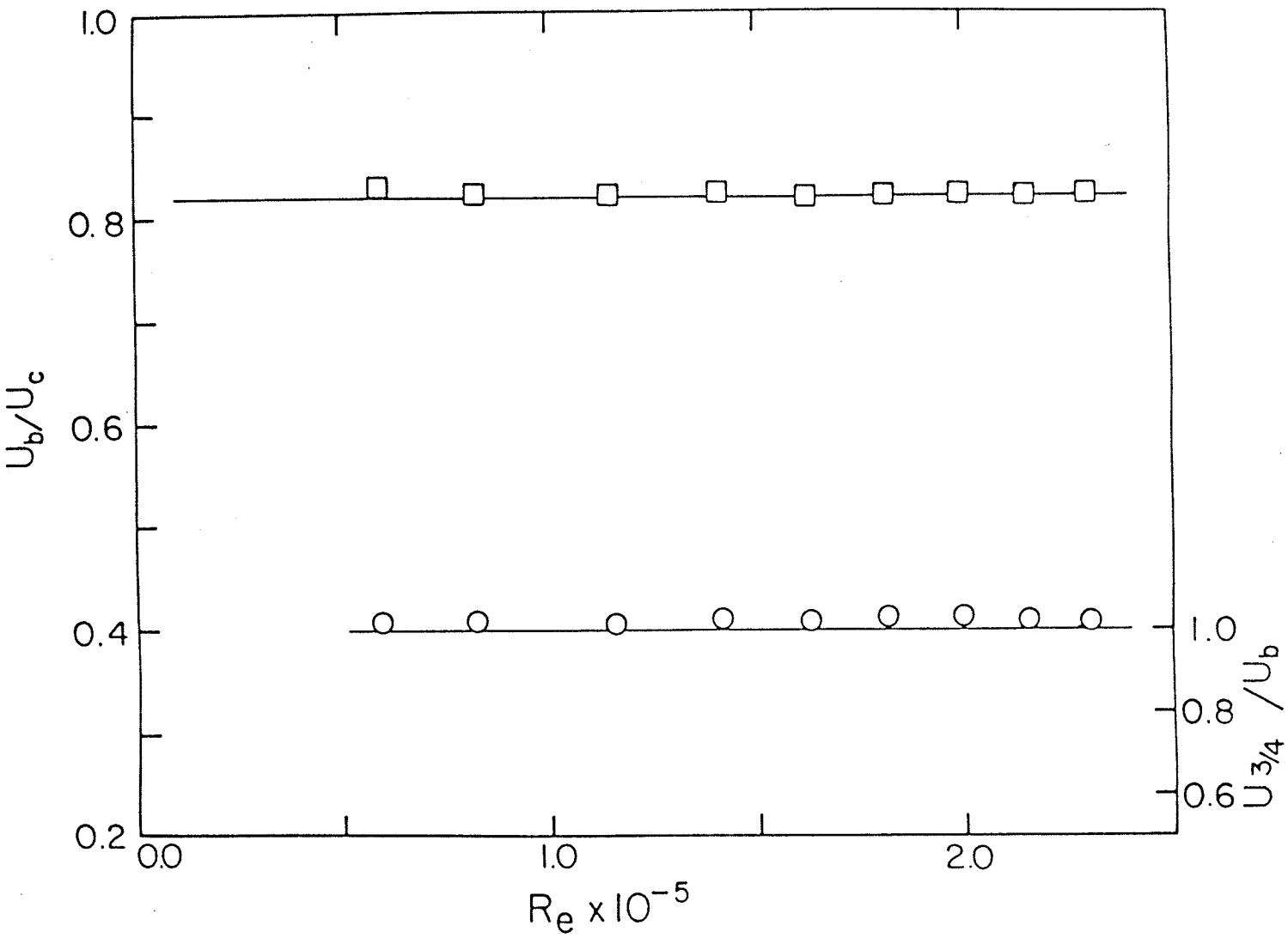

Figure 14. Ratio of U_b/U_c and $U_{3/4}/U_b$

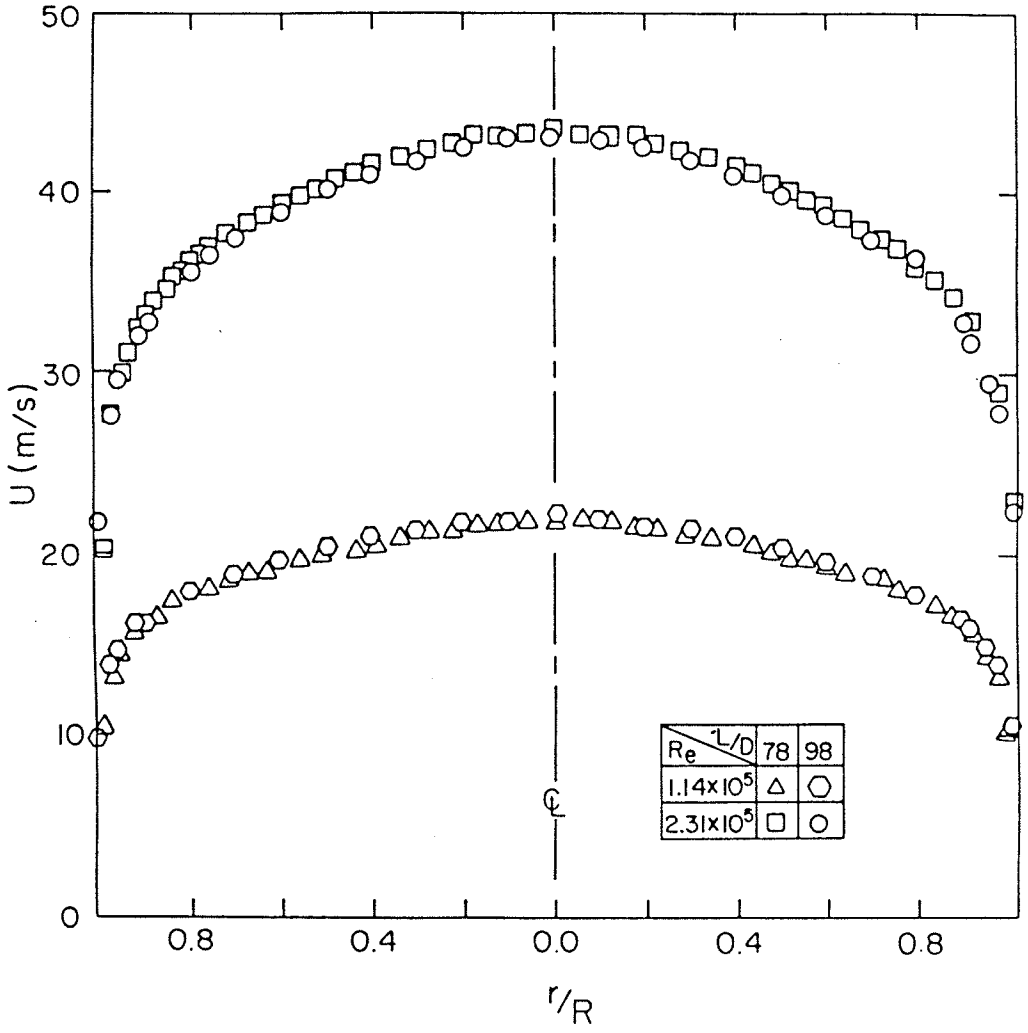

Figure 15. Velocity profile at L/D = 78 and L/D = 98 for Re = 1.14 x 10^5 and Re = 2.31 x 10^5

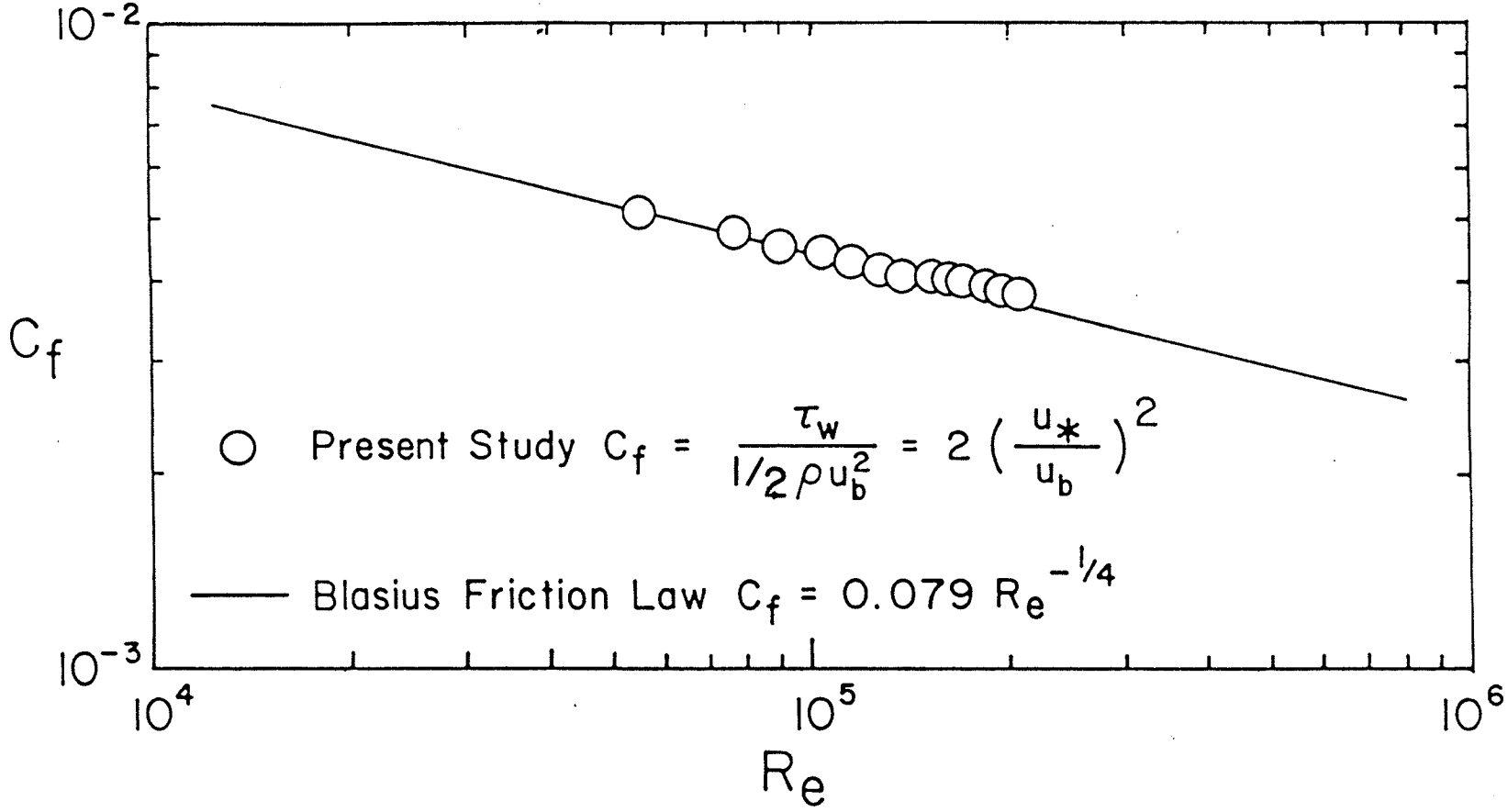

Figure 16. Skin friction coefficient versus Reynolds number

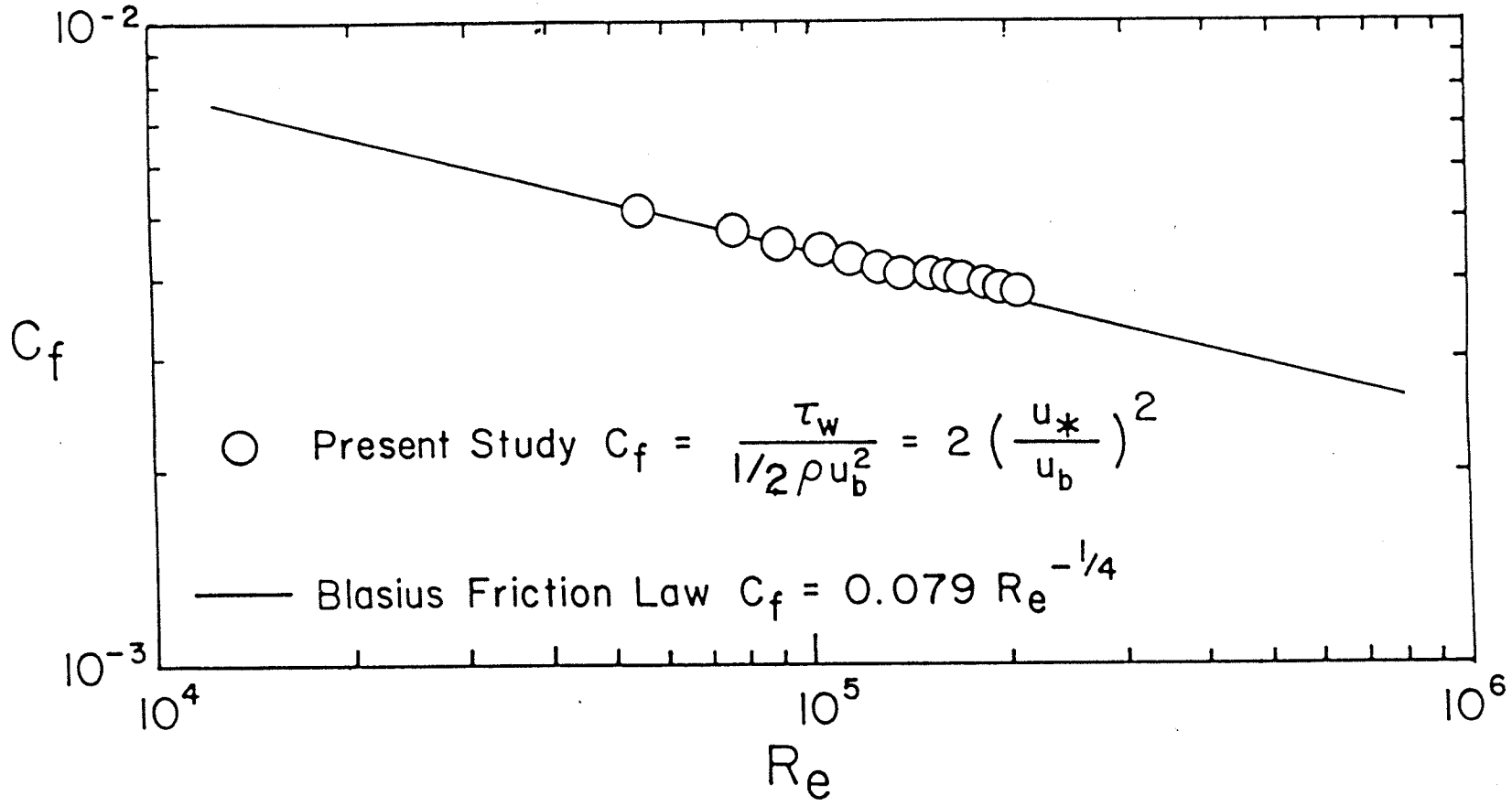

Figure 16. Skin friction coefficient versus Reynolds number

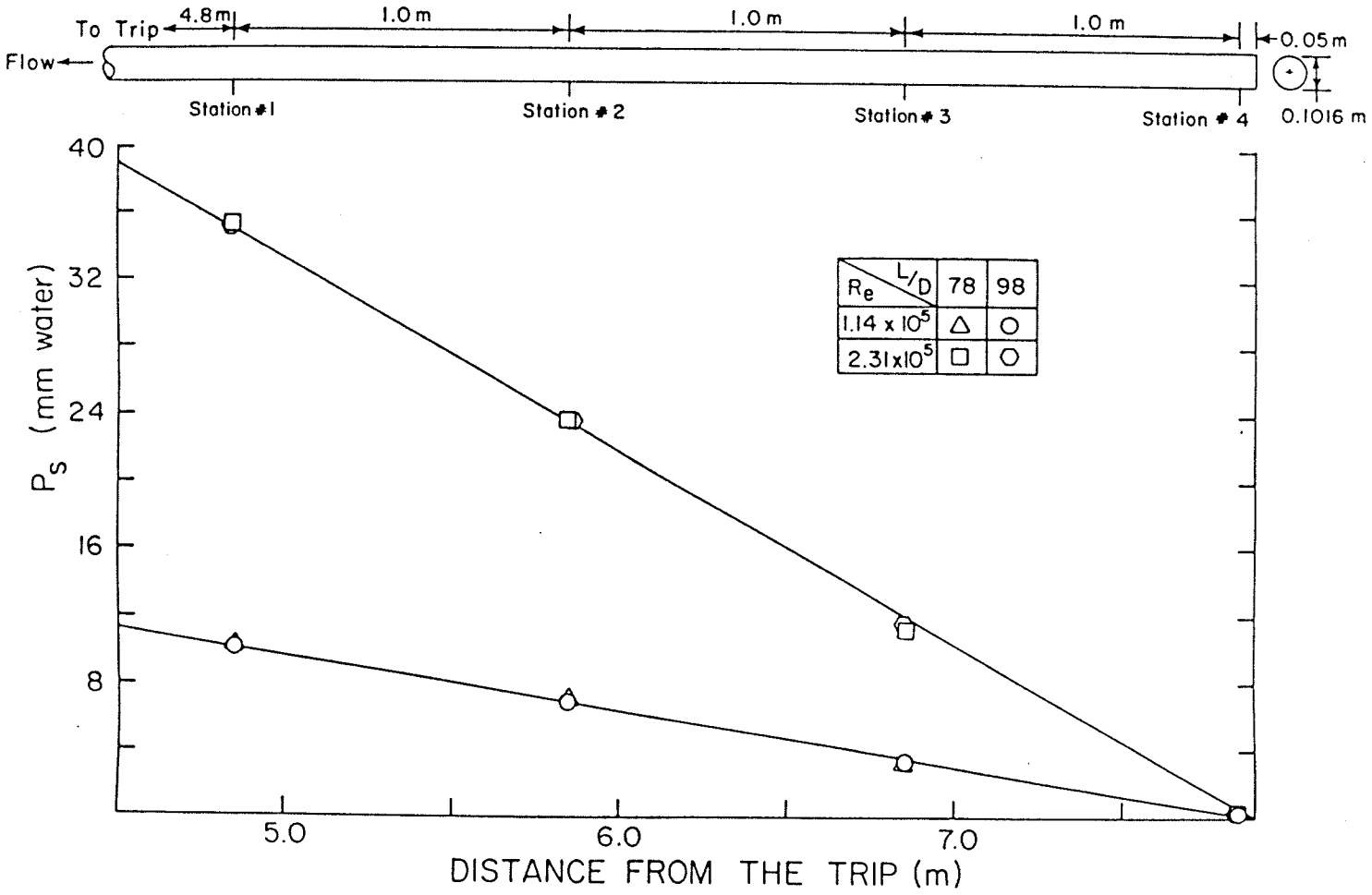

Figure 17. Distribution of static pressure for metal pipes

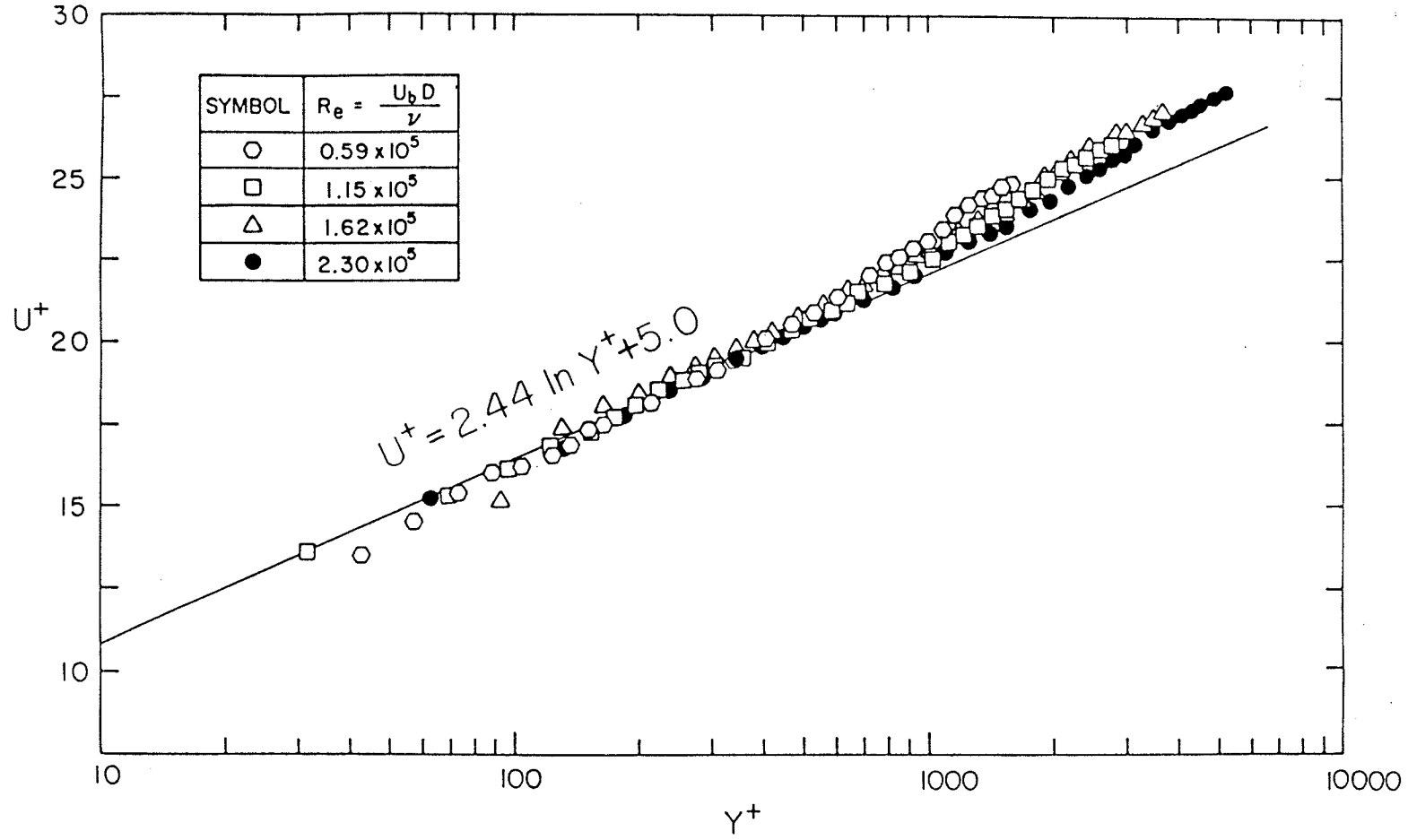

Figure 18. Non-dimensional velocity distribution: plot obtained with pitot tube

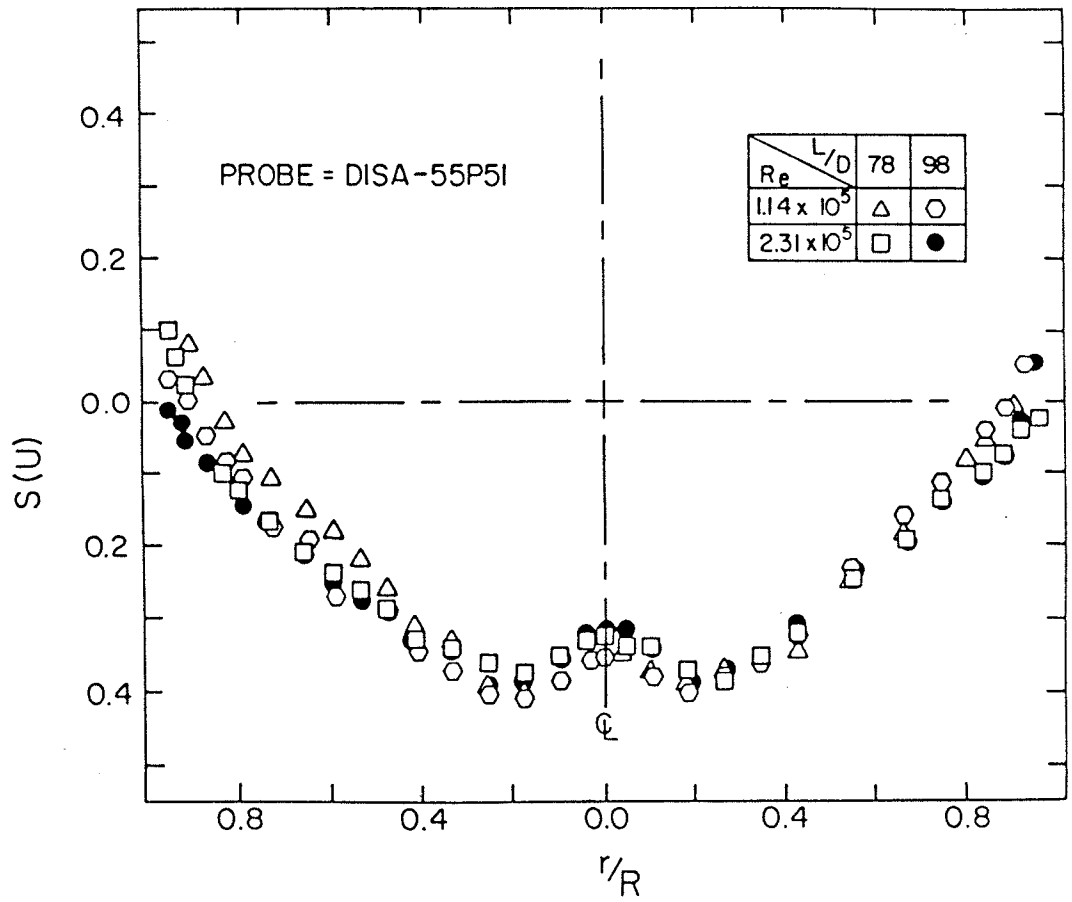

Figure 19. Skewness distribution of the longitudinal velocity, u, $s(u) = \overline{u^3}/(\overline{u^2})^{3/2}$

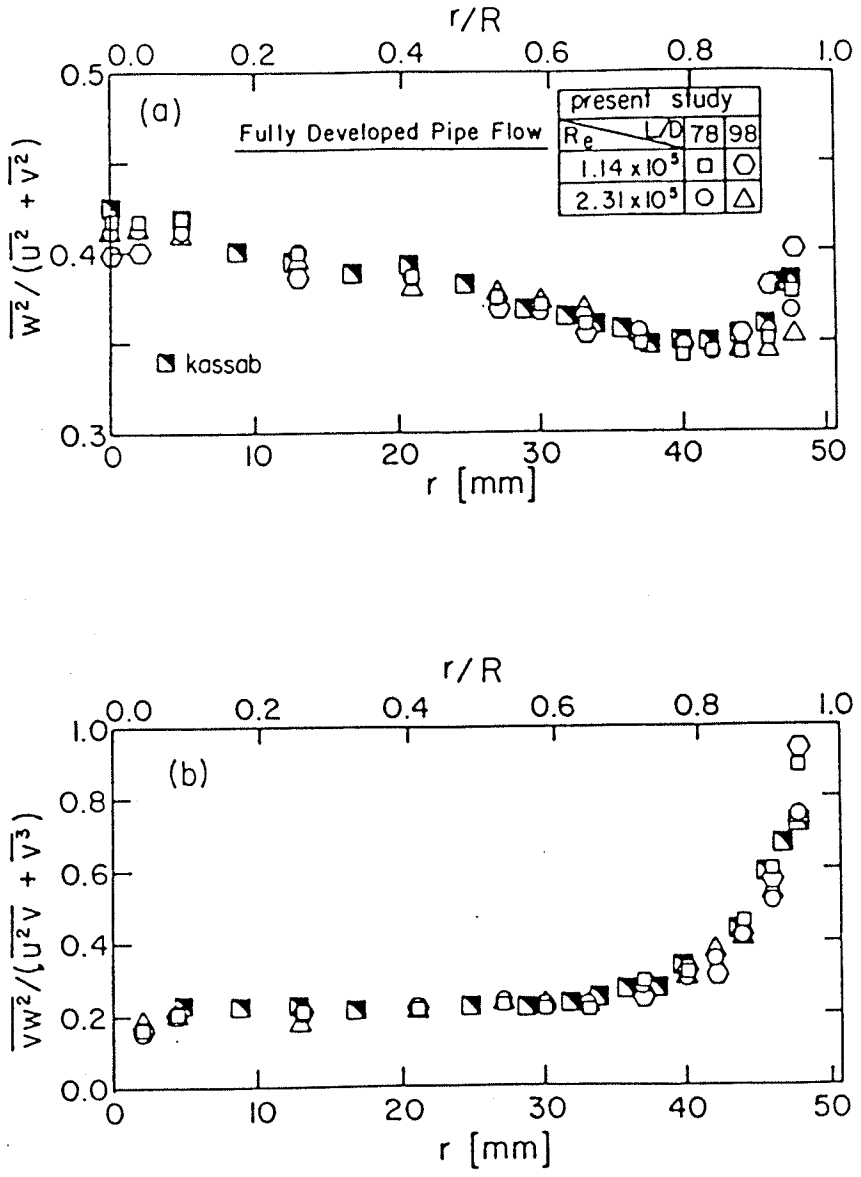

Figure 20: Moments of turbulent fluctuating velocity in fully developed pipe flow

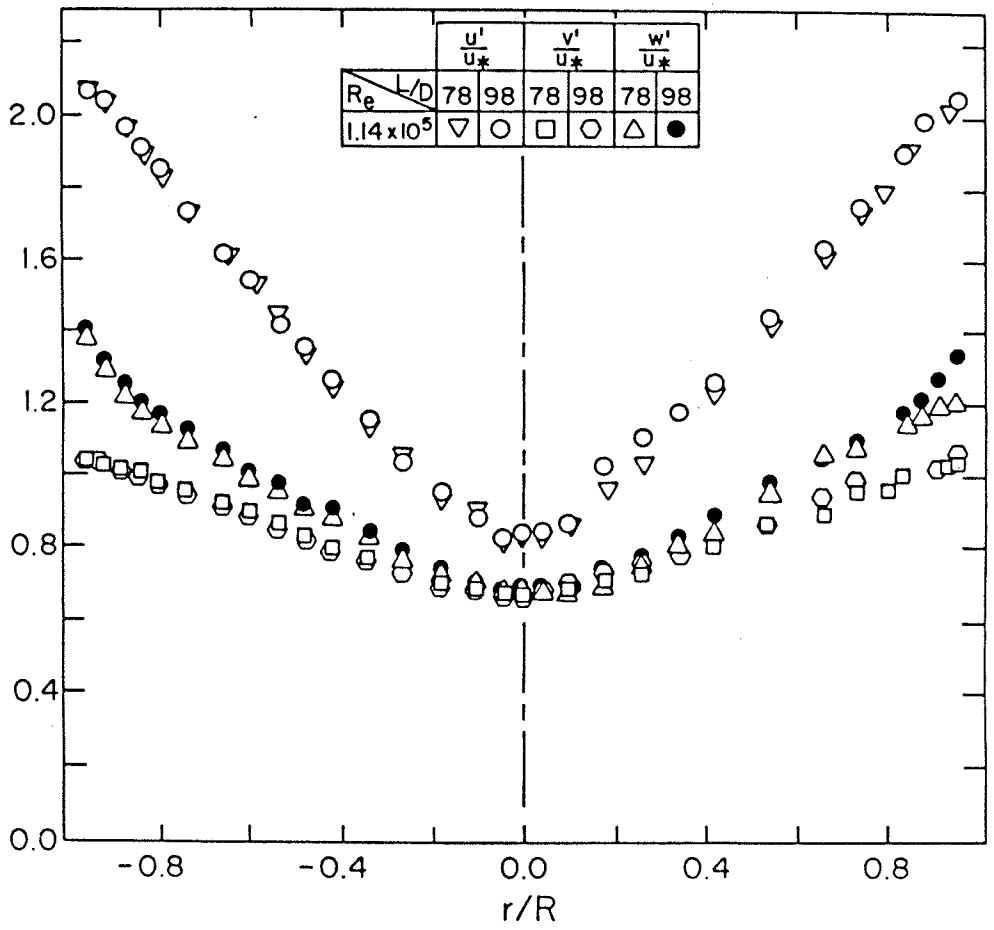

Figure 21. Fluctuating velocity distributions at L/D = 78 and L/D = 98 for Re = 1.14 x 10^5

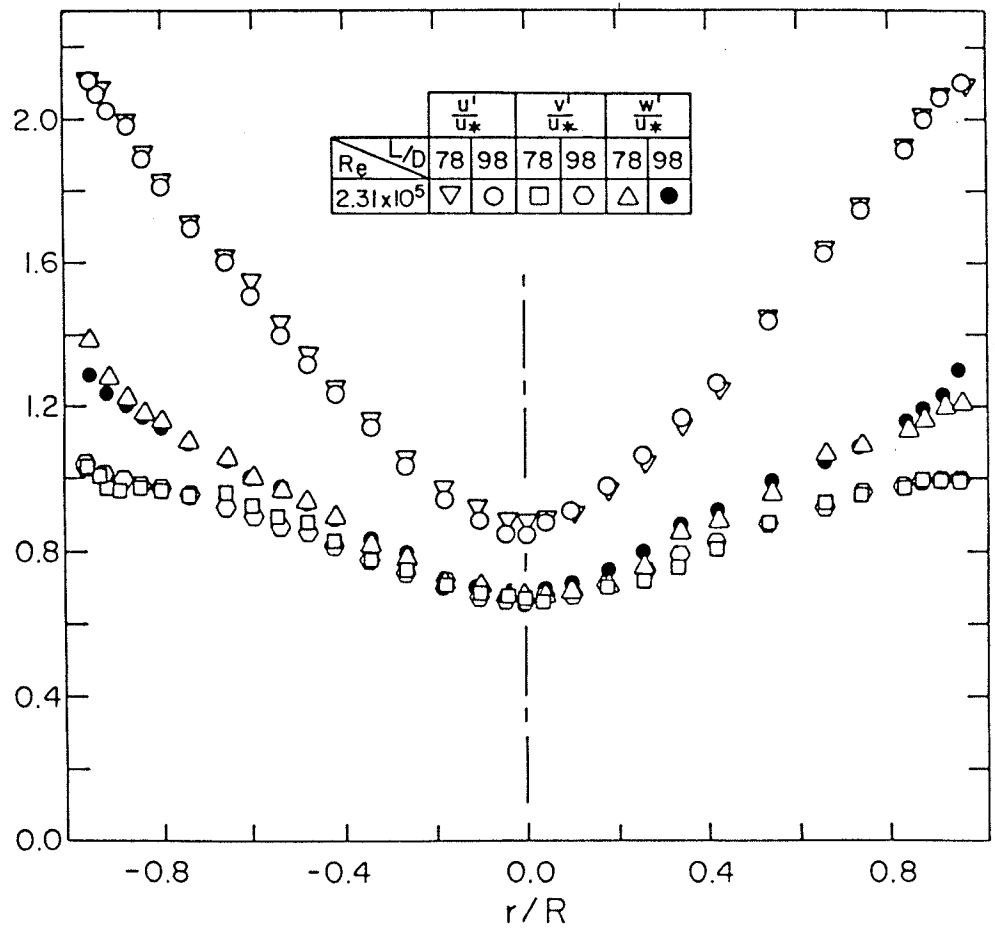

Figure 22. Fluctuating velocity distributions at L/D = 78 and L/D = 98 for Re = 2.31×10^5

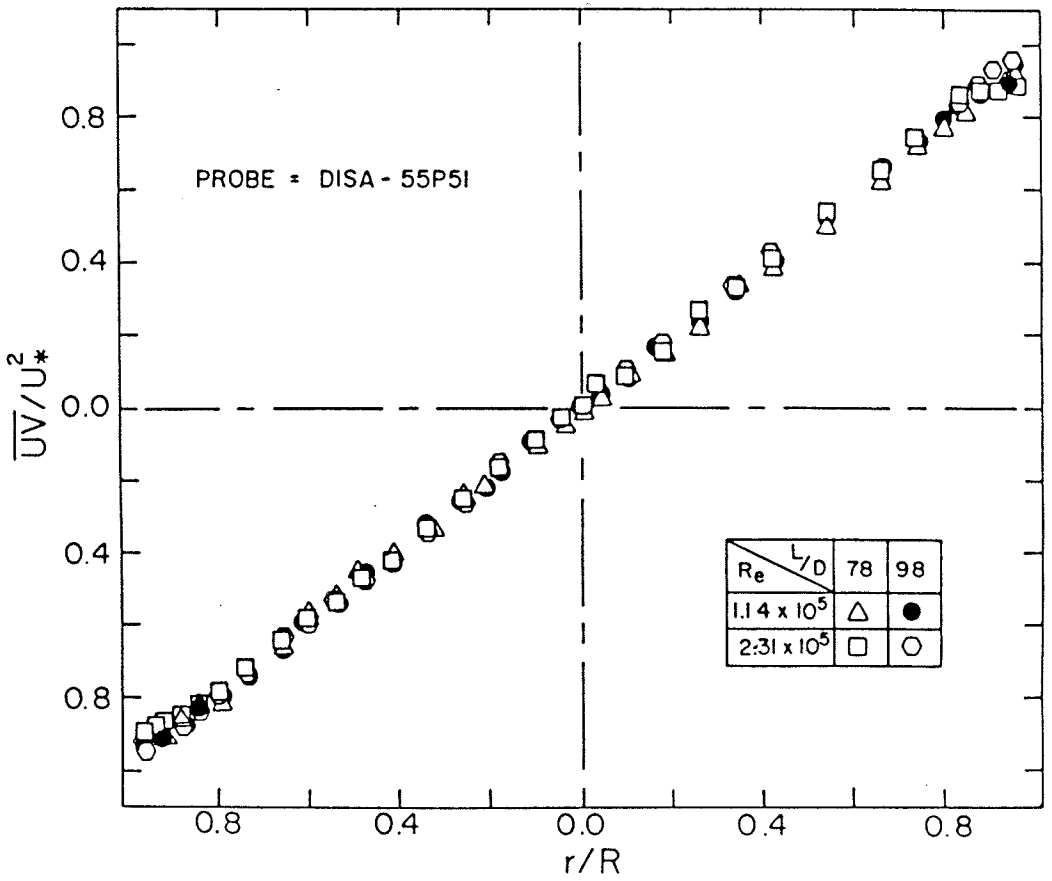

Figure 23. Shear stress measurements at L/D = 78 and L/D = 98 for Re = 1.14 x 10^5 and 2.31 x 10^5

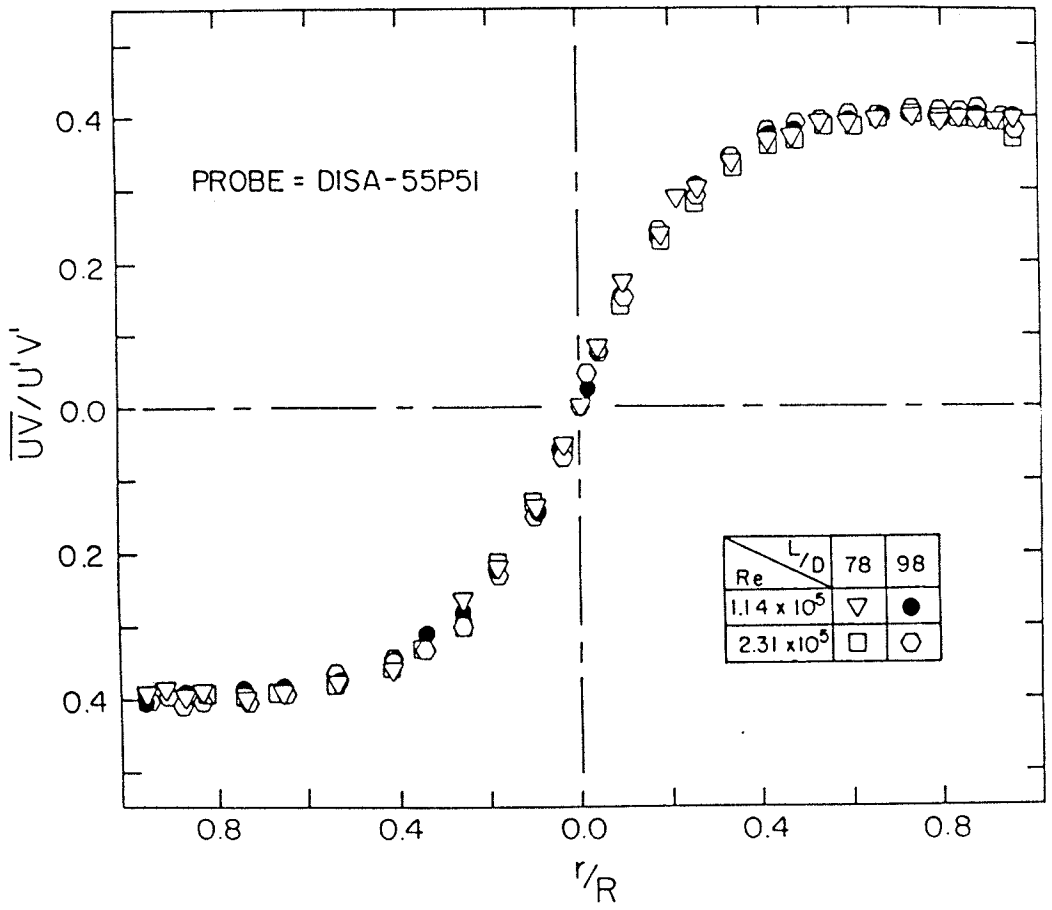

Figure 24. Profile of the correlation coefficient $\overline{uv}/(u' v')$ across the pipe flow

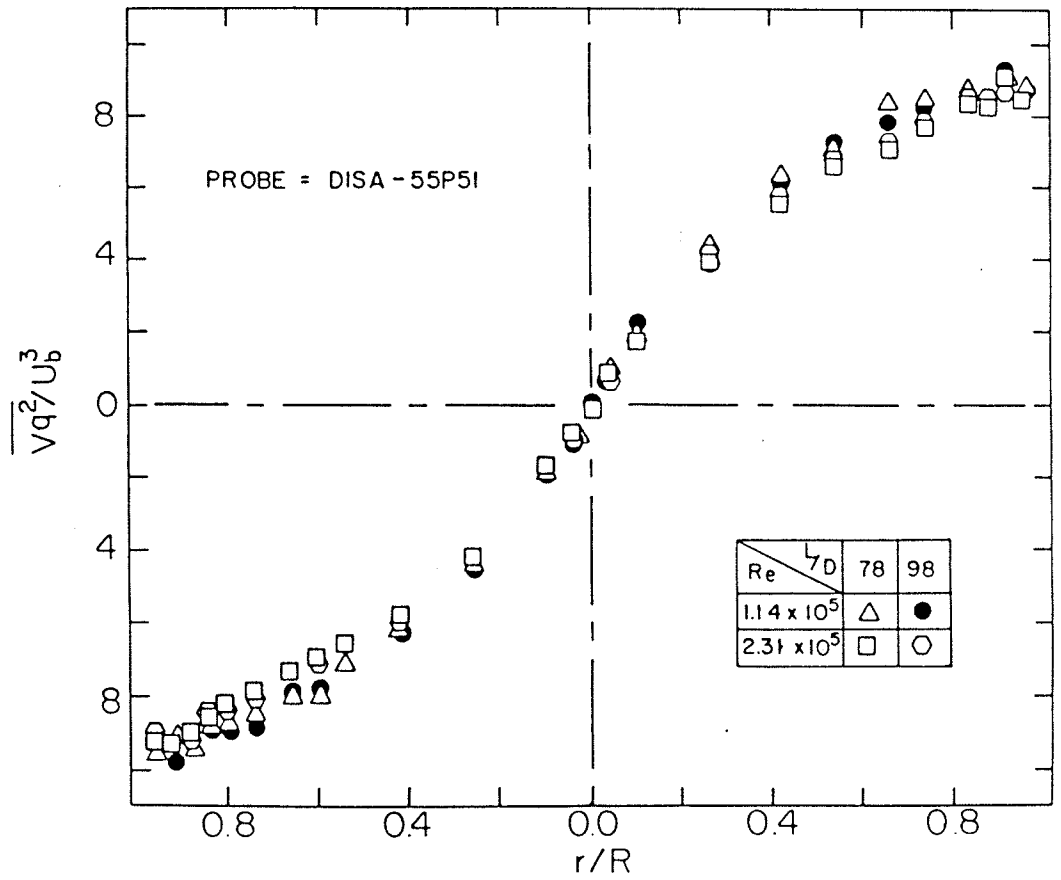

Figure 25. Distribution of $\overline{vq^2}/U_b^3$

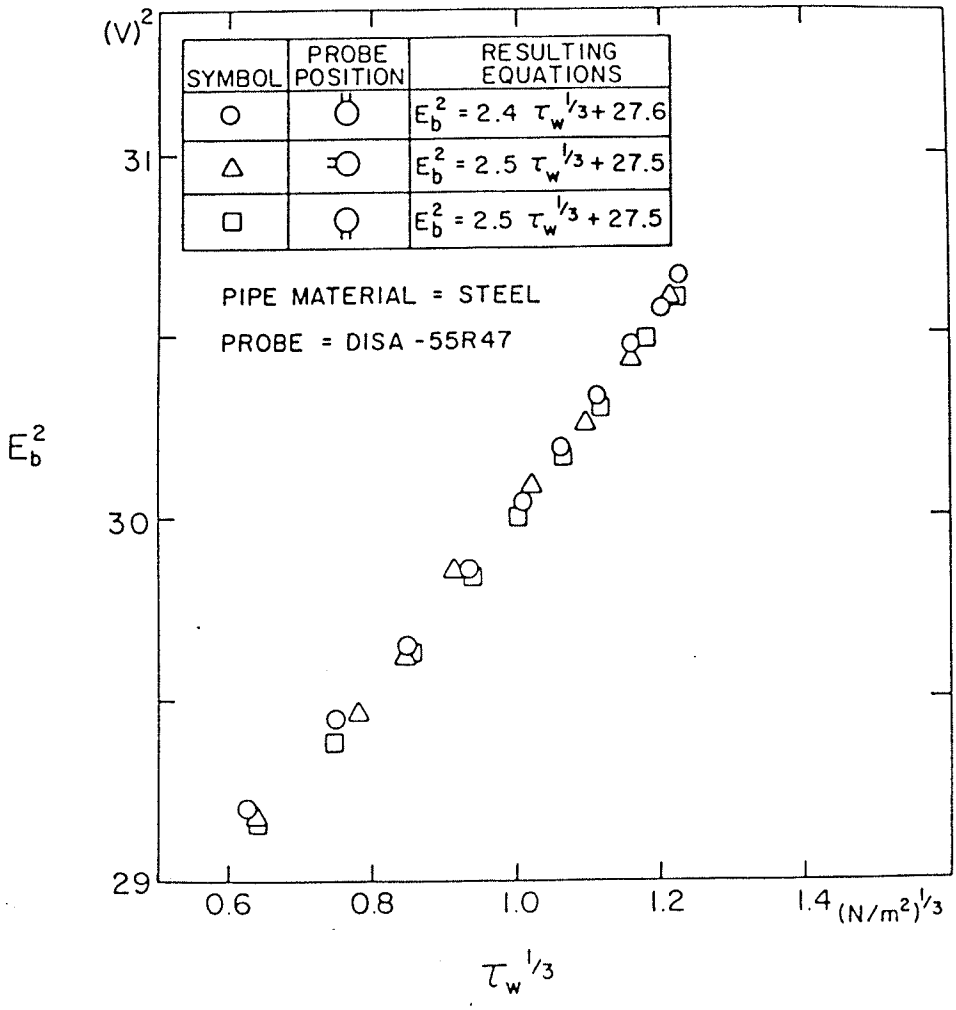

Figure 26. Calibration curve for DISA-55R47 hot-film probe mounted on steel pipe

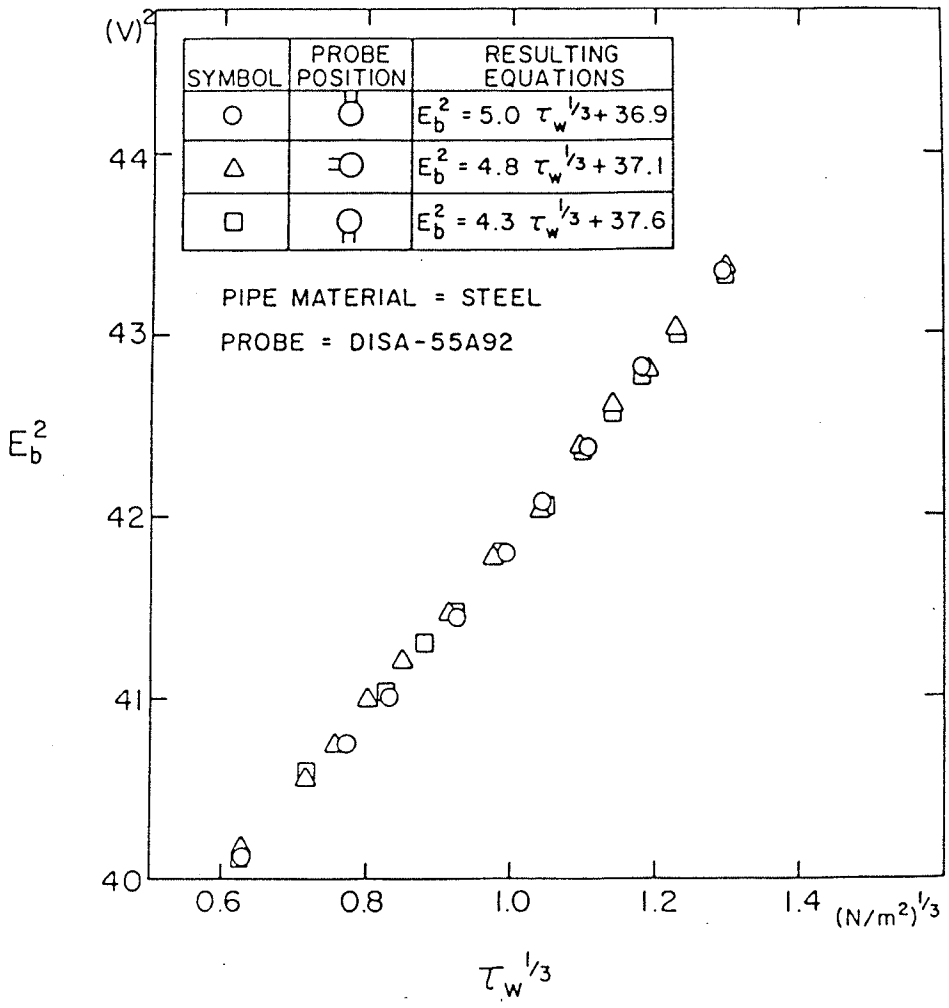

Figure 27. Calibration curve for DISA-55A92 hot-film probe mounted on steel pipe

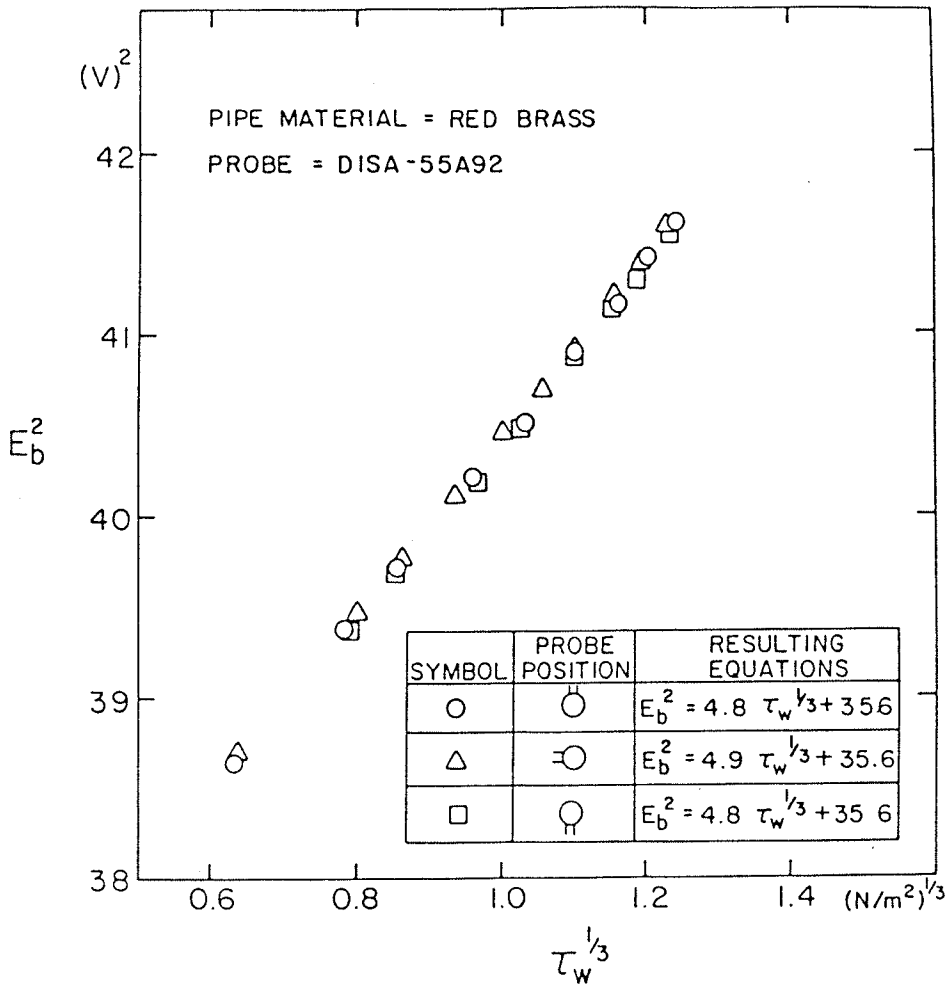

Figure 28. Calibration curve for DISA-55A92 hot-film probe mounted on red brass pipe

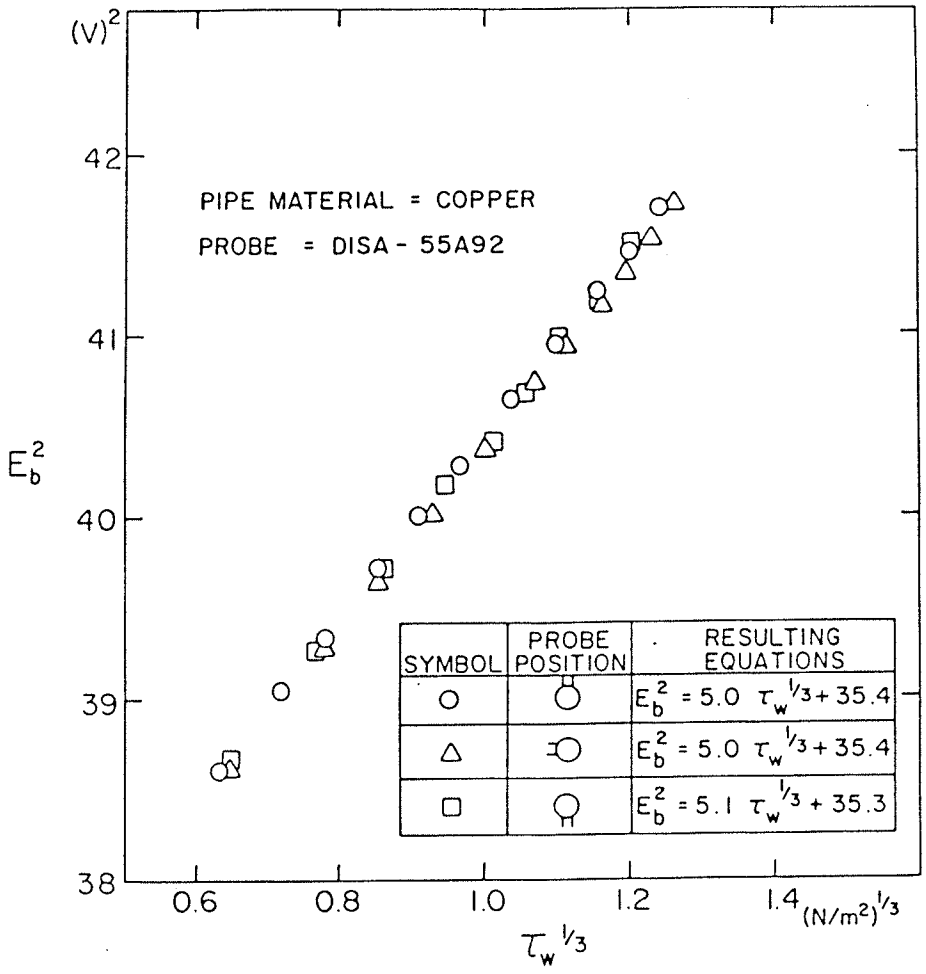

Figure 29. Calibration curve for DISA-55A92 hot-film probe mounted on copper pipe

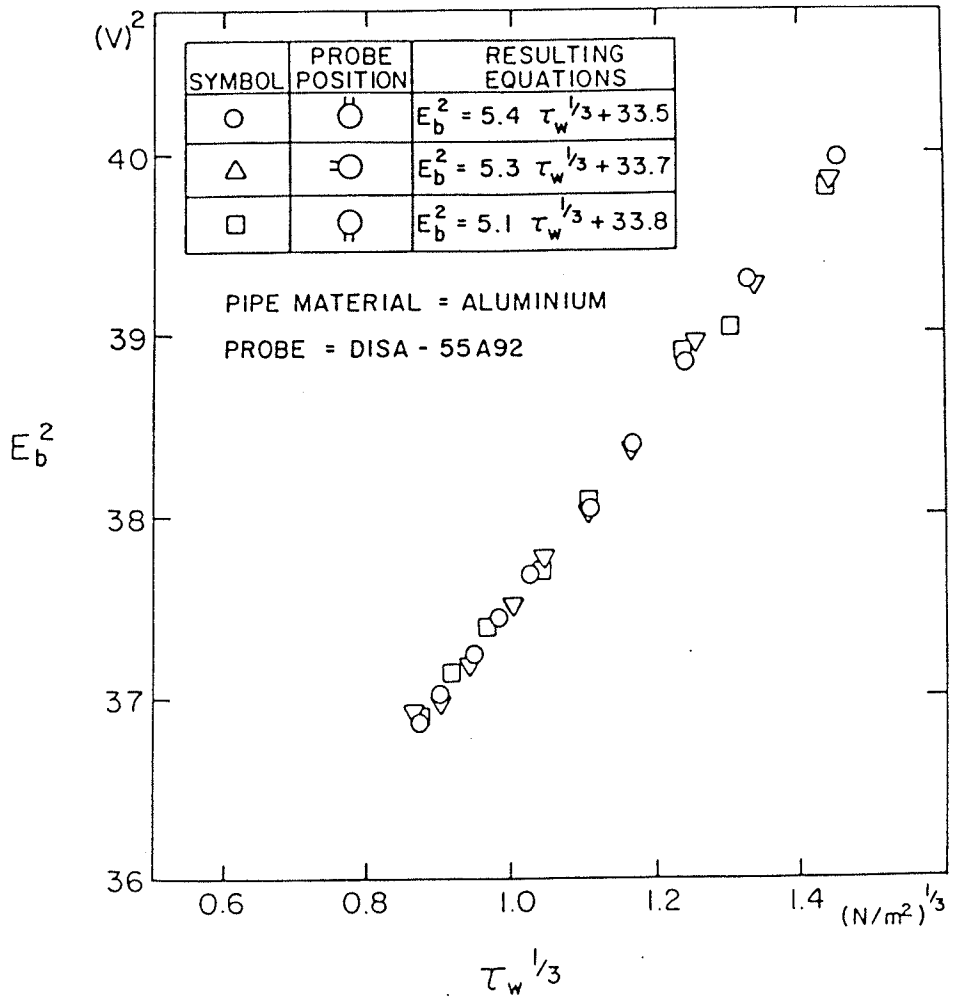

Figure 30. Calibration curve for DISA-55A92 hot-film probe mounted on aluminium

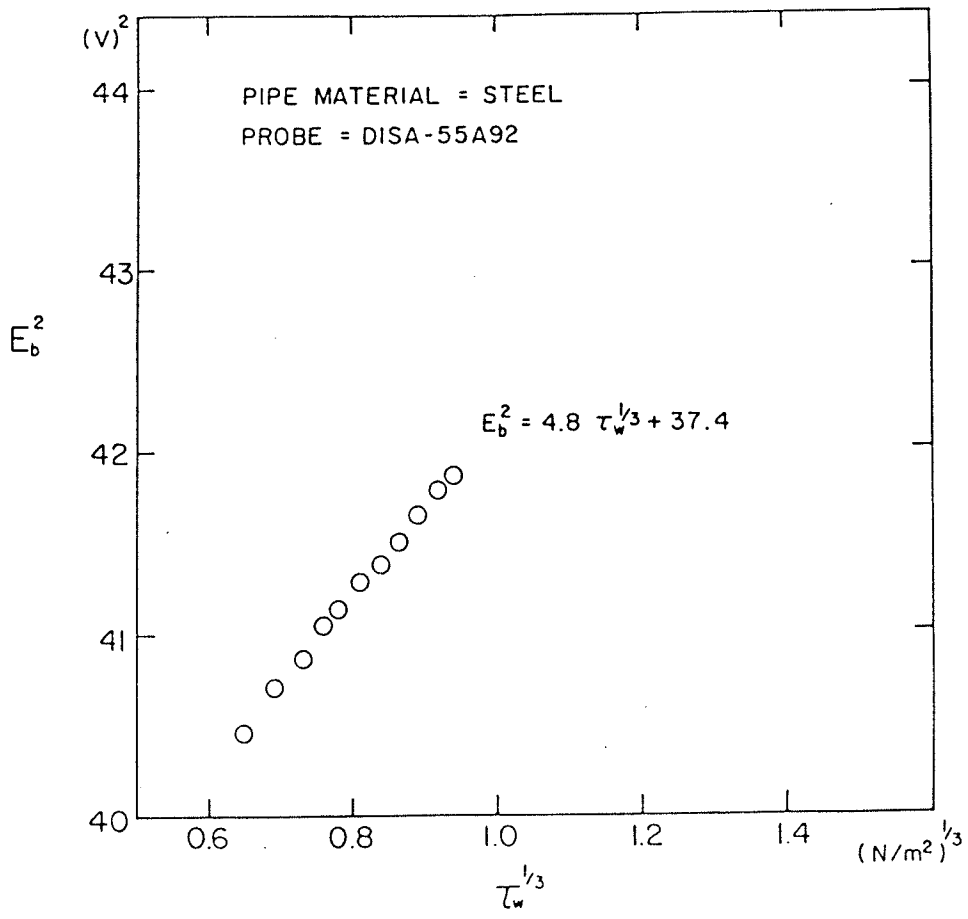

Figure 31. Calibration curve for DISA-55A92 hot-film probe mounted on steel pipe - Test #2

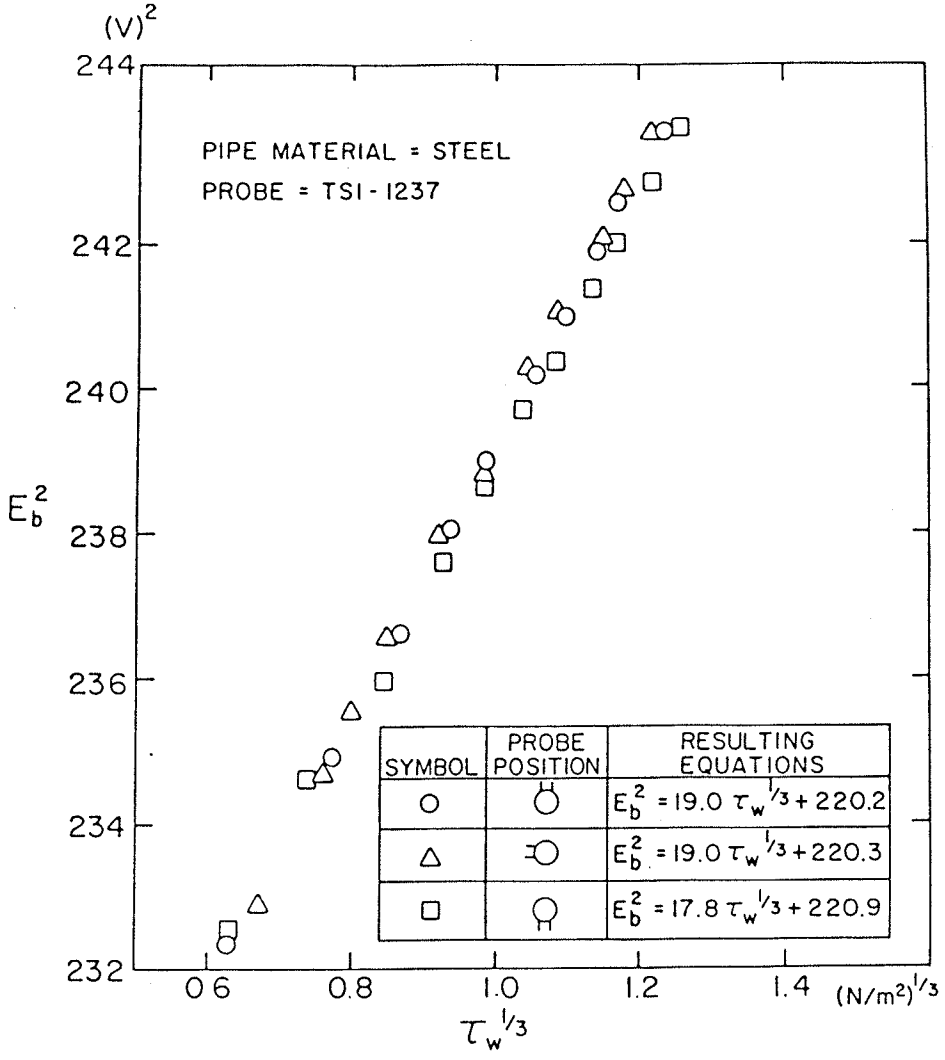

Figure 32. Calibration curve for TSI-1237 hot-film probe mounted on steel pipe

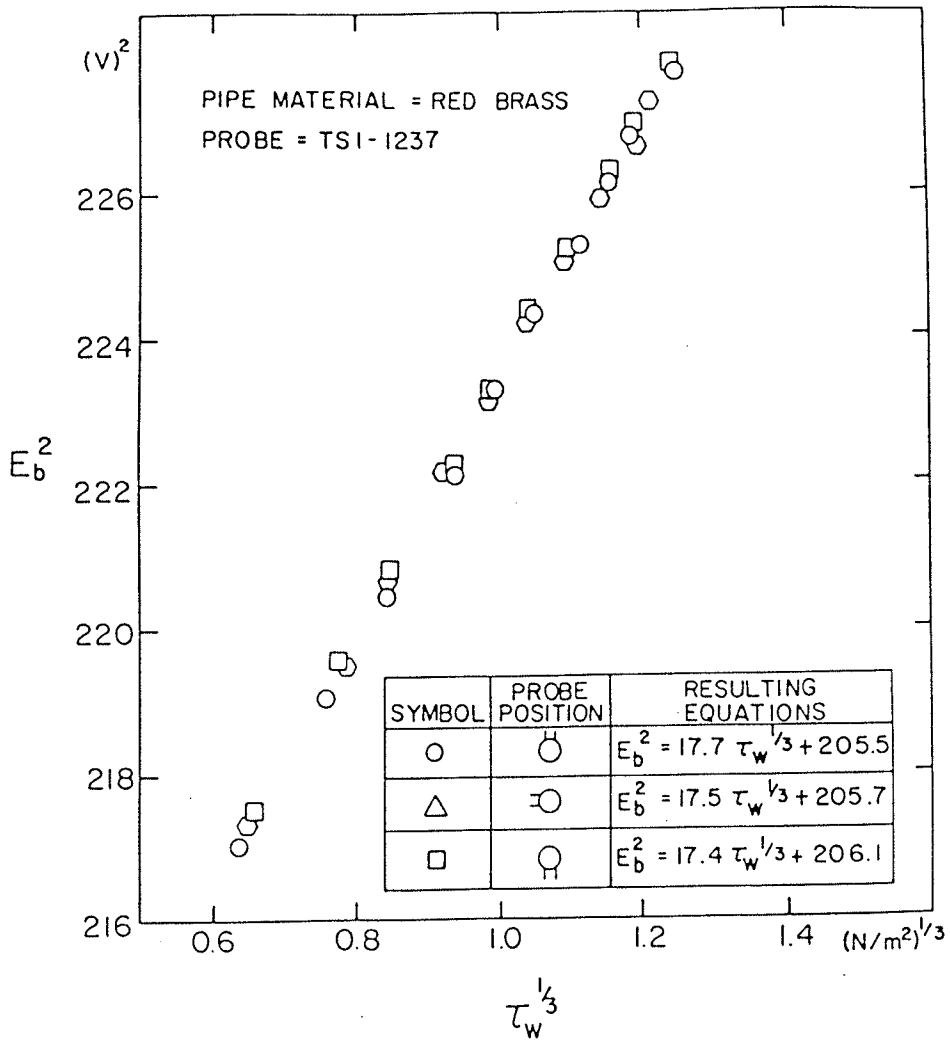

Figure 33. Calibration curve for TSI-1237 hot-film probe mounted on red brass pipe

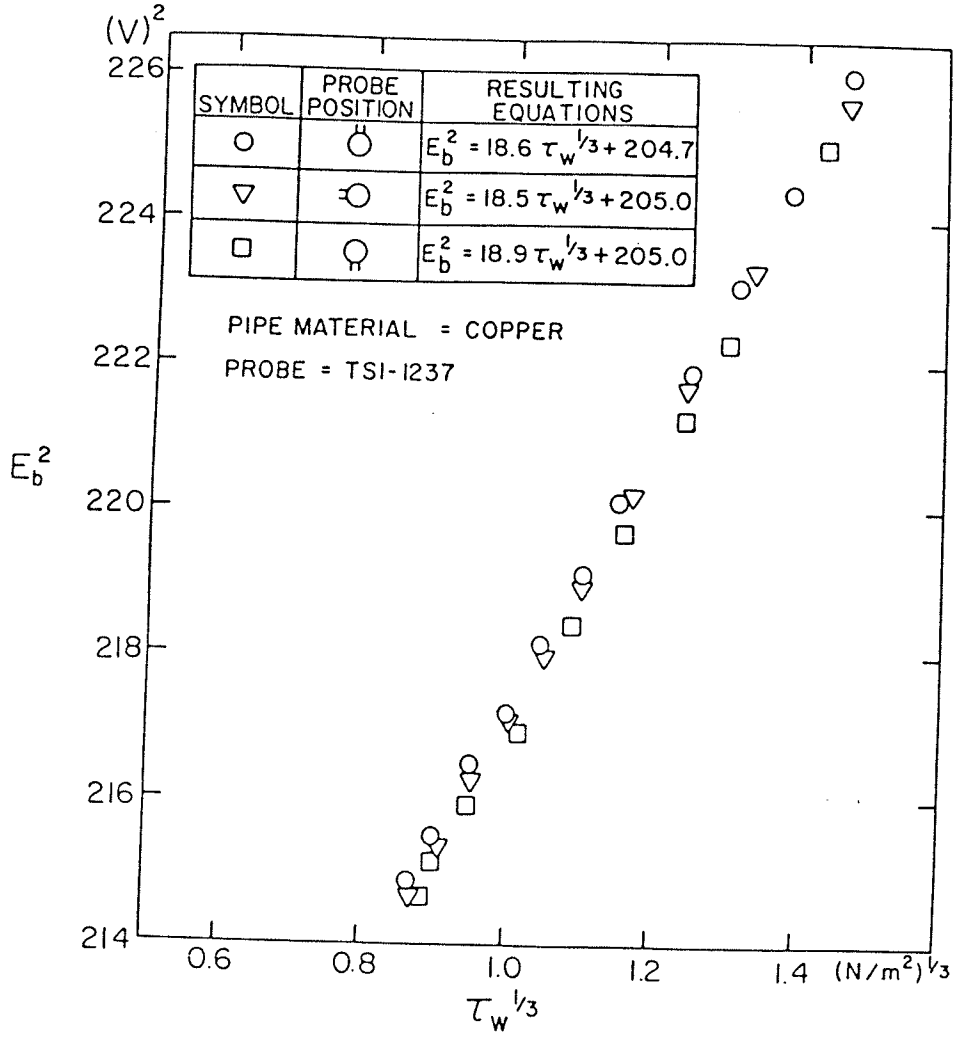

Figure 34. Calibration curve for TSI-1237 hot-film probe mounted on copper pipe

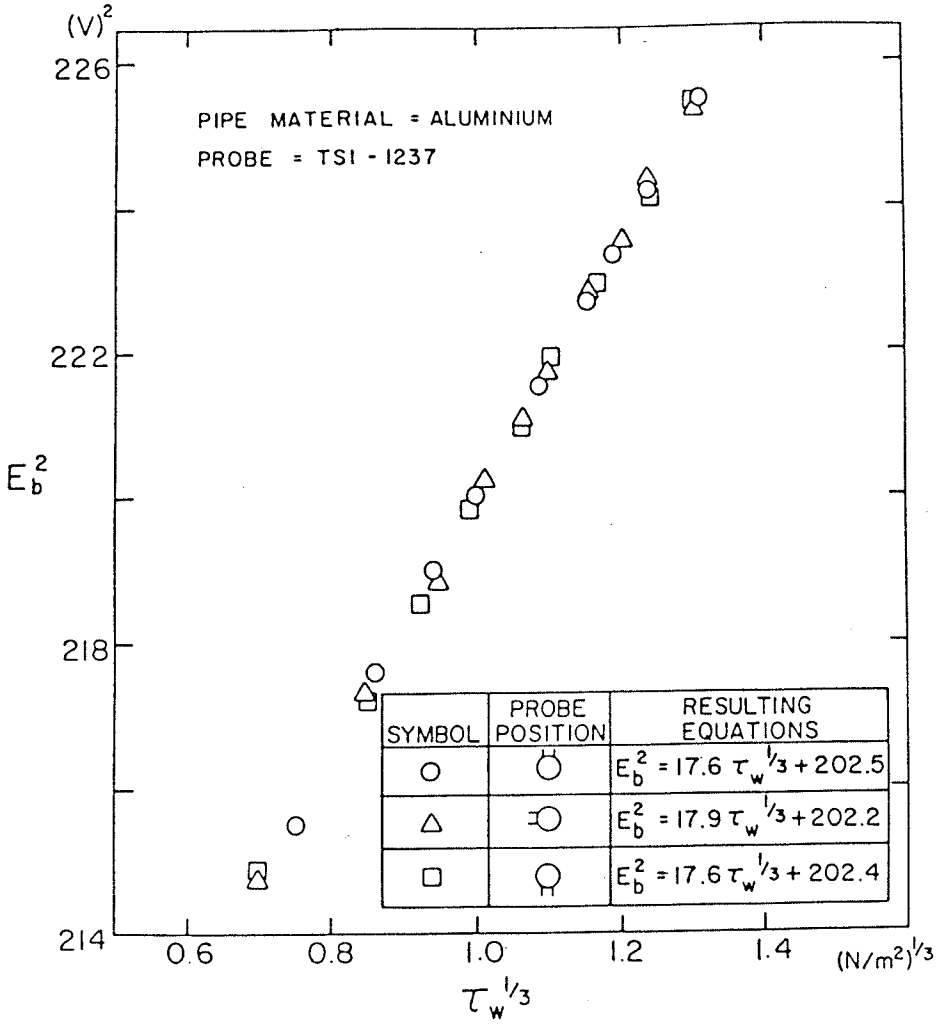

Figure 35. Calibration curve for TSI-1237 hot-film probe mounted on aluminium pipe

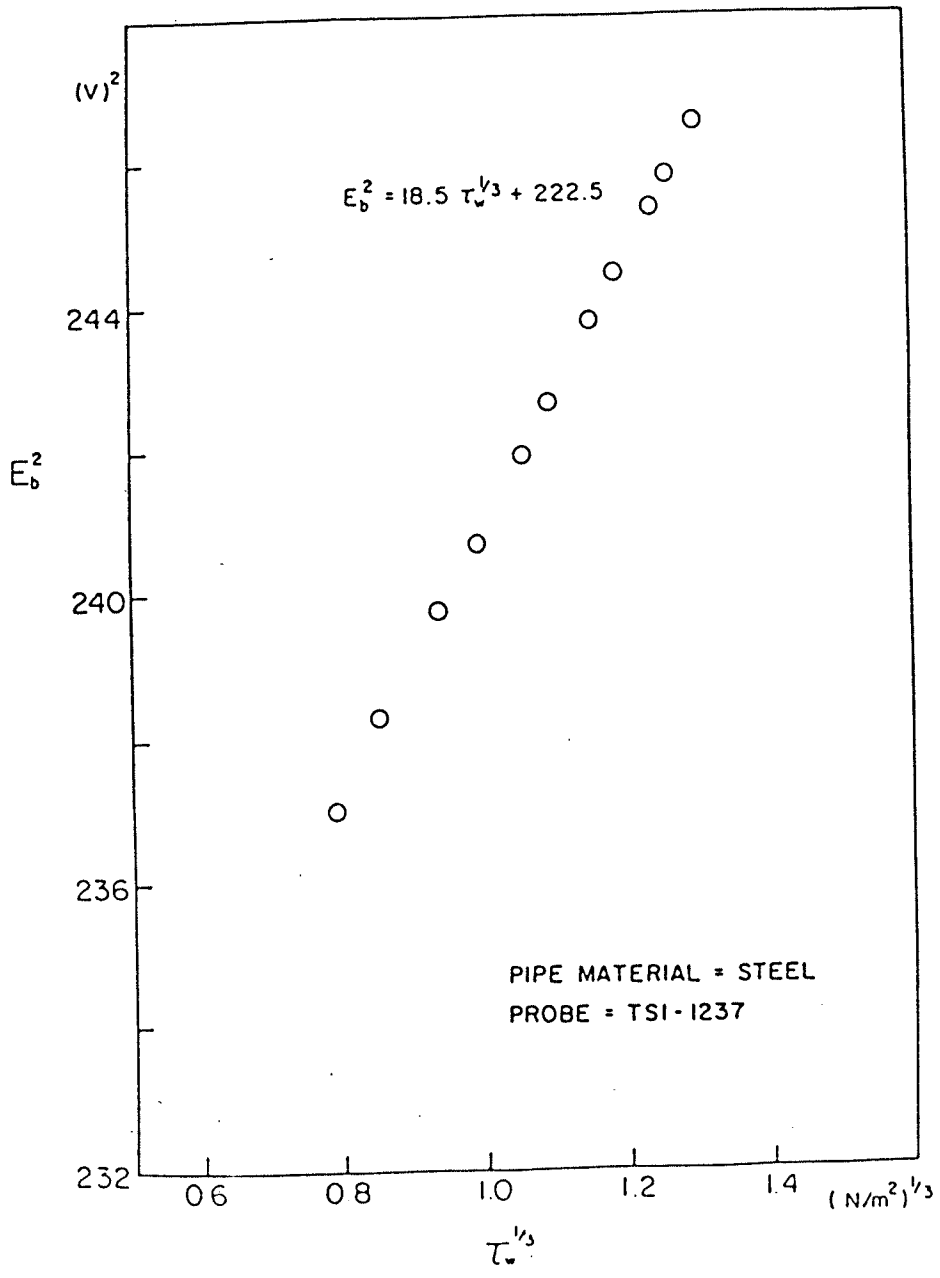

Figure 36. Calibration curve for TSI-1237 hot-film probe mounted on steel pipe - Test #2

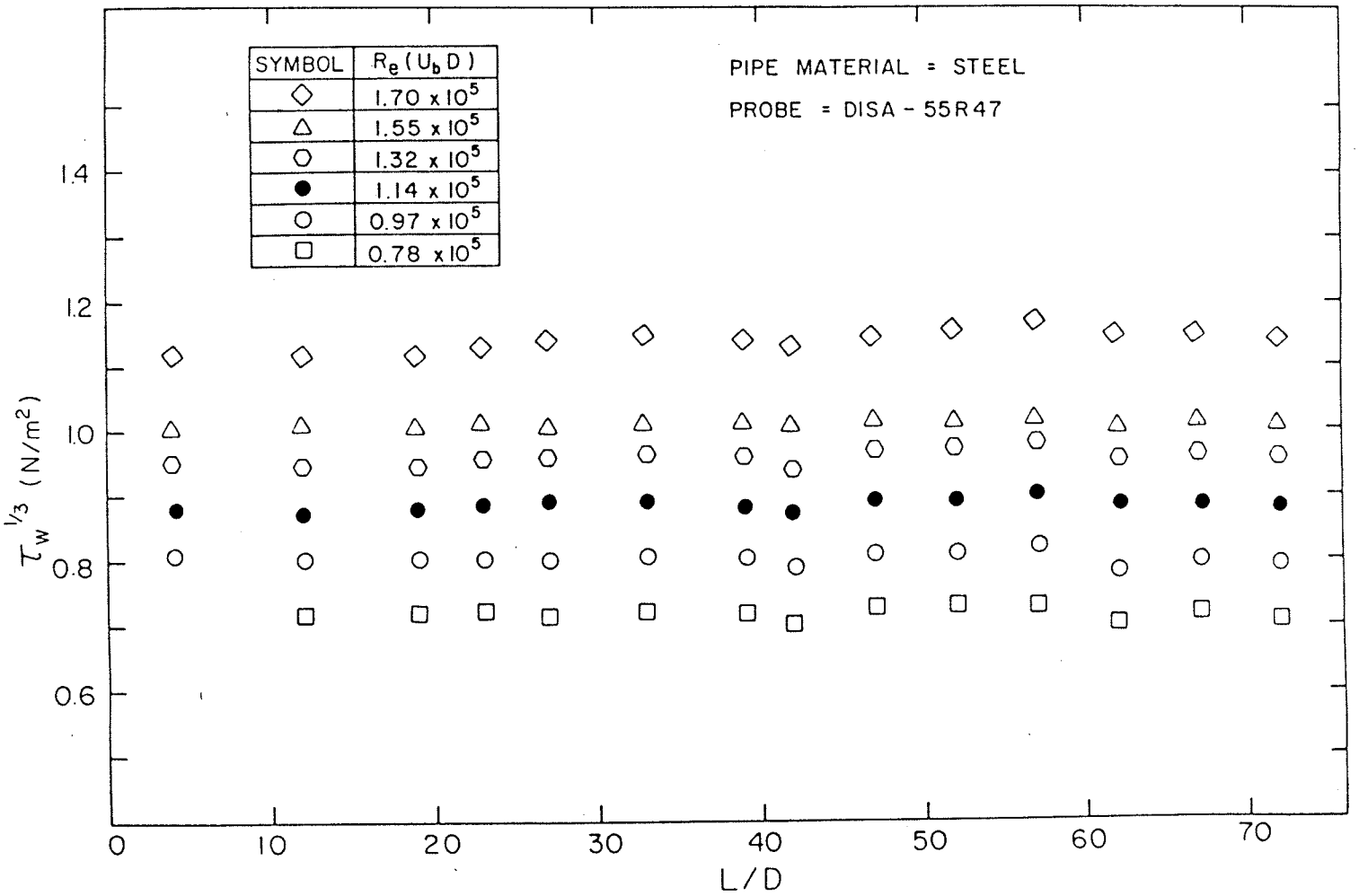

Figure 37. Shear stress distribution along pipe length

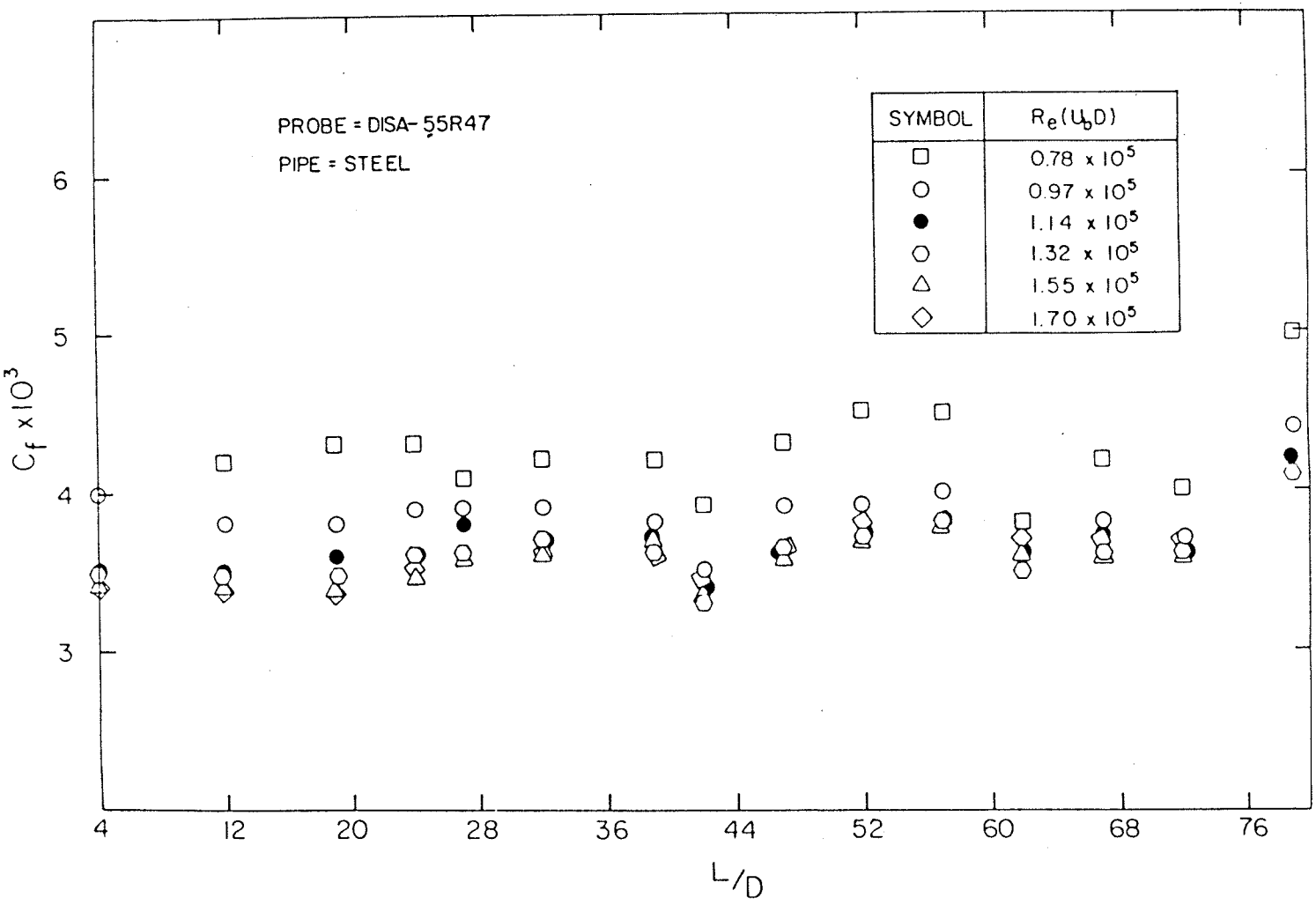

Figure 38. Skin friction distribution along pipe length